A SUBCRITICAL, GAS-COOLED FAST TRANSMUTATION REACTOR WITH A FUSION NEUTRON SOURCE

RADIOACTIVE WASTE MANAGEMENT AND DISPOSAL

KEYWORDS: *transmutation reactor, fast reactor, fusion neutron source*

W. M. STACEY,* V. L. BEAVERS, W. A. CASINO, J. R. CHEATHAM, Z. W. FRIIS, R. D. GREEN, W. R. HAMILTON, K. W. HAUFLER, J. D. HUTCHINSON, W. J. LACKEY, R. A. LORIO, J. W. MADDOX, J. MANDREKAS, A. A. MANZOOR, C. A. NOELKE, C. DE OLIVEIRA, M. PARK, D. W. TEDDER, and M. R. TERRY *Georgia Institute of Technology Atlanta, Georgia 30332*

E. A. HOFFMAN *Argonne National Laboratory, Argonne, Illinois*

Received June 14, 2004
Accepted for Publication October 5, 2004

A design is presented for a subcritical, He-cooled fast reactor, driven by a tokamak D-T fusion neutron source, for the transmutation of spent nuclear fuel (SNF). The reactor is fueled with coated transuranic (TRU) particles and is intended for the deep-burn (>90%) transmutation of the TRUs in SNF without reprocessing of the coated fuel particles. The reactor design is based on the materials, fuel, and separations technologies under near-term development in the U.S. Department of Energy (DOE) Nuclear Energy Program and on the plasma physics and fusion technologies under near-term development in the DOE Fusion Energy Sciences Program, with the objective of intermediate-term (~2040) deployment. The physical and performance characteristics and research and development requirements of such a reactor are described.

I. INTRODUCTION

Advanced reactor concepts that can achieve more efficient electricity production, passive safety, and advanced fuel cycles that better utilize fuel resources and reduce high-level radioactive waste repository requirements are being studied intensively in the U.S. Generation-IV Nuclear Energy System Initiative[1] (GEN IV) and Advanced Fuel Cycle Initiative[2] and in related international activities. In parallel, a research and development (R&D) program is being initiated to further the development of coated fuel particle technology that will enable the achievement of extremely high burnup without fission product (FP) gas release.[3]

Our purpose is to contribute to these ongoing studies by investigating the utilization of the coated fuel particle technology to achieve deep (>90%) burnup of the fissionable transuranic (TRU) content in the spent nuclear fuel (SNF) from commercial light water reactors (LWRs), with minimal or no reprocessing of the coated TRU fuel particle after initial fabrication from LWR SNF. This investigation includes (a) the recovery of TRU from LWR SNF utilizing extensions of proven aqueous separation processes; (b) the design of coated TRU fuel particles and associated fuel elements that are compatible with the fast reactor environment in which they will be used; (c) the preliminary conceptual design of an annular, subcritical, fast He-cooled reactor that will maximize the achievement of deep burnup of the TRU; (d) the preliminary conceptual design of a fusion neutron source to drive the subcritical reactor; (e) the analysis of the nuclear fuel cycle to evaluate the transmutation performance consistent with radiation damage limits; and (f) safety and electrical performance evaluations.

The design process was driven by the objectives of (a) achieving deep TRU burnup with minimal or no reprocessing of the coated TRU fuel particles and (b) using the physics and technology design databases that either exist or are being developed in ongoing R&D programs. A subcritical reactor was chosen to achieve a larger reactivity margin to prompt-critical and to allow the reactivity decrease with burnup to be partially compensated by increasing the neutron source strength, both of which should contribute to the achievement of deep

*E-mail: weston.stacey@nre.gatech.edu

burnup. A fast spectrum reactor was chosen because all of the TRUs have a larger fission-to-capture ratio in a fast spectrum than in a thermal spectrum. A He-cooled reactor was chosen because the United States (Argonne National Laboratory) and France (Commissariat à l'Energie Atomique) are collaborating on the design of a critical He-cooled fast reactor under the GEN-IV program[4] and we make use of certain concepts and technologies that are being developed. However, the high thermal-electrical conversion efficiencies possible with He were not realized in order to avoid the problems associated with the high materials temperatures that would be required. A fusion neutron source was chosen rather than the more extensively investigated accelerator neutron source because it can be designed on the basis of the existing physics and technology databases and because we have the additional objective to evaluate a fusion neutron source for this application. An aqueous fuel-processing system was chosen because of the greater practical experience with it than with other systems.

II. DESIGN CONFIGURATION

A design concept has been developed for a subcritical, fast, He-cooled transmutation reactor fueled with TRUs from LWR SNF. This reactor concept is designated the Gas Cooled Fast Transmutation Reactor (GCFTR). The reactor and associated tokamak fusion neutron source configuration are depicted schematically in Fig. 1. The reactor is annular, with a 5.25-m inner radius, 1-m core thickness, and 3-m height. The annular tokamak plasma neutron source (2.08-m plasma chamber width and 3.5-m height) is located just inside of the annular core, separated by a 2.5-cm-thick first wall attached to the core structure. The core-plasma region is surrounded by a 15-cm-thick reflector, then by a 61-cm-thick shield, and then by a 6-cm vacuum vessel. A set of 16 "D-shaped" toroidal field (TF) magnets are outside the shield, forming a continuous ring 93 cm thick that abuts the shield on the inboard side, as shown, but separated from the shield by a large gap on the top, bottom, and outboard sides where there are also gaps between the discrete coils (gaps and separation not represented in Fig. 1). The inner legs of the TF coils (TFCs) abut a central solenoid (CS) magnet of 70-cm radial thickness, the empty bore of which forms the central magnetic flux core of 66-cm radius.

III. OVERVIEW AND SUMMARY

The design parameters were developed for two coated particle fuel options: the tri-material isotropic (TRISO) coated fuel particle with a TRU kernel surrounded by SiC, C, and ZrC layers embedded in a SiC matrix and the

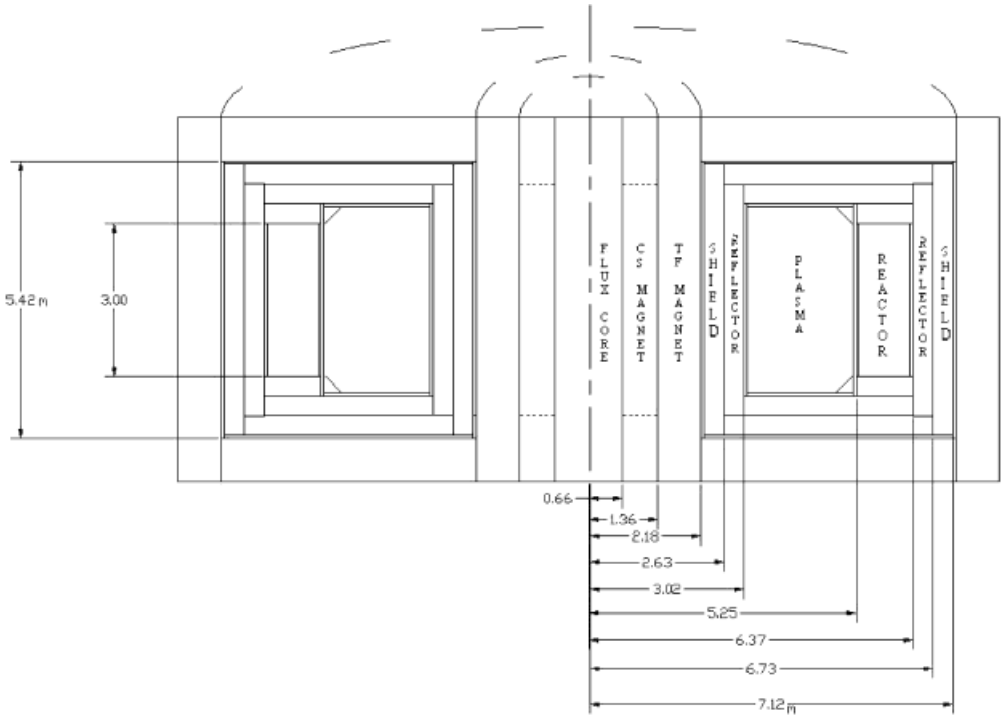

Fig. 1. Schematic and dimensions of the GCFTR.

bi-material isotropic (BISO) coated fuel particle with ZrC and C layers embedded in a Zircaloy matrix. Major parameters of the GCFTR are given in Table I.

III.A. Fuel

Two coated fuel particle concepts were investigated. The dimensions and composition were determined from a trade-off among reactivity, heat removal, and lifetime against FP gas buildup. Design concepts were developed for a TRISO particle and for a BISO particle. The TRISO particle has a TRU kernel (300-μm diameter) surrounded by a 50% porous buffer layer (100 μm) of ZrC to allow for FP recoil and to accommodate FP gas buildup, followed by a structural layer (20 μm) of pyrolytic carbon that prevents chlorine attack of the kernel during the coating process and contains the FPs, followed by a structural layer (25 μm) of SiC that shrinks under irradiation to provide an inward pressure to counteract the FP gas pressure buildup, followed by an outer pyrolytic carbon layer (35 μm) to prevent interaction of the SiC with any metallic cladding material. The BISO particle has a similar kernel and buffer layer followed by a (25-μm) pyrolytic carbon structural layer and then by a (35-μm) ZrC structural outer layer.

It is an objective to achieve very high burnup before loss of integrity of the coated fuel particle or degradation of FP gas containment becomes unacceptable. The TRISO and BISO particles are predicted, based on ORIGEN calculations[5] of FP gas buildup, to reach 155 MPa at 90% FIMA and 180 MPa at 99% FIMA for the maximum predicted fuel centerline temperature of 560°C. For the

TABLE I

Major Parameters of the GCFTR

Parameter	Value
Reactor	
Dimensions (annular)	R_{in} = 5.25 m, R_{out} = 6.37 m, height = 3.0 m
Fuel/He/structure (vol%)	TRISO 60/30/10; BISO 65/25/10
TRU coated particle diameter	TRISO/660 μm; BISO/620 μm
TRU-oxide fuel coated particle/matrix/enrichment	TRISO/SiC/70%; BISO/Zircaloy/60%
TRU fuel mass	TRISO/36 tonnes; BISO/47 tonnes
Maximum k_{eff}	0.95
Maximum T_{fuel}	560°C
He coolant T_{He}, pumping power	T_{in} = 280°C, T_{out} = 480°C, P_{pump} = 0.15 MW
Clad/structural materials	Zircaloy-4/HT-9
Fission power	3000 MW(thermal)
Reflector	
Materials	70% HT-9, 30% He
Thickness	15 cm
Shield	
Materials	40% W, 40% B_4C, 20% He
Thickness	61 cm
Plasma	
Major and minor radii, elongation	R_o = 4.15 m, a = 1.04 m, κ = 1.75
Plasma current	7.15 MA
Fusion power/neutron source rate	50 MW/1.8 $\times 10^{19}$ s^{-1} to 200 MW/7.1 $\times 10^{19}$ s^{-1}
Fusion gain ($Q_p = P_{fus}/P_{plasma\ heating}$)	180 MW(thermal)/62.5 MW(thermal) = 2.9
Superconducting magnets	
Conductor	Nb_3Sn cable-in-conduit
Field CS, TFC, on center of plasma	12.4 T, 11.8 T, 6.3 T
Divertor	
Materials	W tiles on Cu bond to CuCrZr, He cooled
Heat flux	$\leq$2.0 MW/m^2
First Wall	
Materials	Be coated on HT-9, He cooled
Neutron wall load (14 MeV)	$\leq$0.85 MW/m^2
Heat flux	$\leq$0.23 MW/m^2

particles described above, with an oxygen "getter" (ZrC) in the buffer region, a void region of only 1.8 times the kernel volume was used in order to increase reactivity. The operational pressure limit due to the compressive yield strength of SiC for the TRISO particle is 345 MPa, and the similar limit for the BISO particle is 352 MPa. These limits correspond to fuel centerline temperature limits of 1700 and 1520°C at 90 and 99% FIMA, respectively, for the BISO particle and to fuel centerline temperature limits of 1690 and 1510°C at 90 and 99% FIMA, respectively, for the TRISO particle. The tensile strength of the pyrolytic carbon layer is less than the limit of 200 MPa.

There are some data on irradiation of TRISO and BISO particles.[6] Examination of the particles irradiated in the Peach Bottom reactor at temperatures of 1200 to 1400 K to a fast (>0.18-MeV) neutron fluence of 1.3×10^{25} n/m^2 found a failure rate of 1.4×10^{-6}. More recent results from coated particle fuel development programs in the United States and Germany have achieved burnups as large as 80% FIMA and fast neutron fluences as large as 1.2×10^{26} n/m^2 at irradiation temperatures of 800 to 1350°C. End-of-cycle (EOC) release-to-production-rate ratios of the FP ^{85m}Kr varied from O(10^{-4}) to O(10^{-6}) for the higher FIMA U.S. experiments but were O(10^{-7}) to O(10^{-9}) for the O(10% FIMA) German experiments. By comparison, it is our objective to irradiate the TRU coated particle fuel in the GCFTR to 90 to 99% FIMA, corresponding to fast neutron fluences of $\sim 5 \times 10^{27}$ to 1×10^{28} n/m^2.

A number of fuel element configurations (pebbles, plates, pins, canisters, compacts) were considered for combining the coated particles and a matrix material (SiC with the TRISO particles, Zircaloy with the BISO particles). For the purpose of thermal and neutronics analyses, we selected a fuel pin clad with Zircaloy containing a uniform mixture of the coated fuel particles in the matrix material.

III.B. Reactor Core

An annular core geometry was chosen for compatibility with the geometry of the fusion neutron source, the parameters of which determined an inner radius $R_{core}^{in} = 5.25$ m and a height of 3 m. A core thickness of 1 m was chosen on the basis of neutronics analysis, as described below, resulting in an outer core radius of $R_{core}^{out} = 6.37$ m, including structural walls of 6 cm on each side. This core is surrounded on the upper, lower, and outboard sides first by a reflector (HT-9, He) and then by a shield (W, B_4C, He). On the inboard side of the reactor is the plasma chamber (neutron source) followed by a reflector and shield.

The thermal analysis was performed for Zircaloy-clad pins in which the BISO fuel particles were uniformly homogenized in the Zircaloy matrix material. A configuration with fuel pins 0.60 cm in radius with a gap of 0.005 cm and a 0.057-cm-thick cladding was chosen for the analysis. At 3000 MW(thermal) total reactor power uniformly distributed in the fuel pins, the average volumetric heat source is $q''' = 42.2$ MW/m^3, which was used in the thermal analysis. With a He mass flow rate of 2870 kg/s, the He coolant entered at 280°C and exited at 481°C, the maximum clad temperature was 513°C (well below the 1845°C melting point for Zircaloy), the maximum homogenized fuel centerline temperature was 560°C, and the He pumping power was 0.15 MW. A heat transport analysis of an individual coated fuel particle with a local heterogeneous heat deposition rate of $q''' = 63.1$ MW/m^3 and using the temperature from the homogenized calculation as a boundary condition on the fuel particle predicted only a 0.5°C increase in the kernel above the homogenized value, so that the maximum centerline temperature in the particle was 561°C (well below the 2000+°C melting point for TRU oxides). Based on this thermal analysis, it was concluded that a He coolant volume percent ≥25% would be adequate for heat removal under normal operating conditions.

Both oxide-dispersion-strengthened (ODS) (melting point 650°C) and ferritic (melting point 550°C) steel were considered for the structural material. A ferritic steel typified by HT-9 was chosen because of the better existing database. Both steels and Zircaloy (melting point 1845°C) were considered for the cladding material, and the Zircaloy was chosen because of its much higher melting point in comparison with HT-9 steel. The radiation damage limit of HT-9 steel is 80 to 150 dpa (Ref. 7), corresponding to a fast neutron fluence of 1.5×10^{23} to 3×10^{23} n/cm^2. The radiation damage limit of Zircaloy is known to be at least 20 dpa, corresponding to a fast neutron fluence of 1×10^{22} n/cm^2, but it may be much longer because of annealing. Using the GCFTR value of the fast (>0.1-MeV) neutron flux of 2×10^{14} n/cm^{2}s, these fluences correspond to a lifetime of 23 to 48 effective full-power years (EFPY) for the HT-9 structure and at least 3.2 EFPY for the Zircaloy cladding. With a 30-EFPY lifetime of the GCFTR (40 yr at 75% availability), the HT-9 structural material might need to be replaced once. The lifetime of the Zircaloy cladding (and matrix material) will affect the determination of a consistent fuel cycle and fuel residence time.

The GCFTR must produce the tritium consumed by the fusion neutron source. We envision placing LiO_2 pins in the reflector region surrounding the core and plasma for this purpose.

III.C. Reflector and Shield

As mentioned above, the reactor is surrounded first with a (70%HT-9, 30%He) reflector to return escaping neutrons and then with a (40%W, 40%B_4C, 20%He) shield to protect the superconducting magnets. In addition to the reflector and shield, a first wall modeled as 2.5 cm of (40%HT-9, 40%He, 20%Be) and a (HT-9) vacuum vessel

located between the reflector and shield and modeled as 6 cm of HT-9 were included in the shielding calculation. The limiting components of the toroidal magnets are the insulator, which has a 10^9-rad limit for glass-epoxy insulator, and the Nb_3Sn superconductor, which has a fast neutron fluence limit of 10^{19} n/m^2 (Ref. 8). Monte Carlo calculations[9] of the detailed reactor, plasma chamber first wall, reflector, vacuum vessel, shield, and magnet geometry indicated that a 15-cm reflector plus a 61-cm shield would result in a cumulative insulator radiation dose and superconductor fast neutron fluence after 40 yr of operation at 75% availability that would satisfy these limits. The total nuclear heating rate in the toroidal magnets was calculated to be 139 kW, removal of which would require 1.94 MW of cooling power.

III.D. Fusion Neutron Source

The plasma parameters of the tokamak fusion neutron source were based on a normalized $\beta_N = 2.0\%$ and a confinement multiplier $H = 1.0$ relative to IPB98$(y,2)$ energy confinement scaling.[10] With an aspect ratio of 4, a design point that satisfies the radial build constraints on flux core radius, magnet thicknesses, and reflector plus shield thickness has a major radius of 4.15 m. The corresponding plasma current and energy amplification factor are 7.15 MA and $Q_p = 2.9$, respectively. This reference operating point with $\beta_N = 2.0\%$ provides a fusion neutron source rate of 6.4×10^{19} n/s at 180-MW fusion power. Lower neutron source rates down to 1.8×10^{19} n/s at 50 MW may result from operating at lower values of β_N, and higher neutron source rates up to 7.1×10^{19} n/s at 200 MW may be obtained by operating at higher values up to $\beta_N = 2.5\%$. With a bootstrap current fraction of 0.35, a current drive efficiency $\gamma_{CD} \approx 0.5\,[10^{20}$ m^{-2} amps/watt (A/W)] is required for steady-state operation at the reference operating point (values up to 0.45 have been achieved to date).

The International Thermonuclear Experimental Reactor (ITER) superconducting magnet system design[11–13] was adapted for the GCFTR. The CS has a flux core radius $r_{fc} = 0.66$ m and a radial thickness of $\Delta_{OH} = 0.70$ m. The conductor design is of the cable-in-conduit type with Nb_3Sn operating at a maximum field of 12.4 T to provide 86.3 start-up volt-seconds. The TFC system consists of 16 coils with a cable-in-conduit Nb_3Sn conductor operating at 11.8 T to provide a TF on axis in the plasma of 6.3 T. The radial thickness of the TFC is conservatively chosen as 0.93 m, although a smaller thickness seems feasible.

The ITER divertor and first-wall designs[14] were also adapted for the GCFTR. The surface of the vertical targets and dome consists of tungsten tiles backed with a layer of copper that is bonded to a CuCrZr alloy matrix. The ITER divertor design was modified to accommodate He coolant (instead of H_2O) by encasing the void space behind the vertical targets and dome to form a coolant manifold and by adding cooling fins on the non-plasma-facing surfaces. The divertor targets will need to be replaced several times during the GCFTR lifetime because of erosion.

The first wall consists of 2-cm-thick HT-9 plates coated on the plasma-facing side with 0.5 cm of Be. Circular coolant channels 1 cm in diameter are located in the HT-9 at the Be-HT9 interface. The first wall is combined with the surface of the contiguous reflectors or reactor core. Over the 40-yr design lifetime of the GCFTR operated at 180 MW fusion power and 75% availability, the HT-9 first wall would accumulate 7.45×10^{23} n/cm^2 fast neutron fluence. With a radiation damage fast fluence limit of 1.5×10^{23} to 3.0×10^{23} n/cm^2 for HT-9, two to five first-wall replacements would be required over the GCFTR lifetime.

III.E. Fuel Processing and Fabrication System

Systems for separating the TRU in LWR SNF and for fabricating it into coated particle fuel have been identified. The uranium (99.995%) is first removed from the SNF using a uranium extraction (UREX) process. The remaining 0.005% of the uranium, the TRU, and the FPs are then treated with a TRU extraction (TRUEX) process and a TRU/lanthanide separation step to remove virtually all of the FPs (Refs. 15 and 16), which are sent to a high-level-waste repository. The TRU emerging from the TRUEX process (including 0.005% of the uranium and virtually all of the TRUs) is then fabricated into coated TRU fuel particles. The heavy metal composition of the "TRU" emerging from this process is (U-0.43%, Np-4.32%, Pu-84.91%, Am-10.21%, Cm-0.13%).

The fabrication process starts with evaporation of the TRU stream, which is then passed through a calciner to form a mixture of actinide oxides. Finally, a ZrC buffer layer and the pyrolytic carbon and ZrC (BISO) or pyrolytic carbon and SiC (TRISO) layers are coated onto the particles. Less than 0.1% TRU loss is assumed during the fabrication process.

Although an objective of this study is to investigate obtaining sufficiently high (>90% FIMA) TRU burnup without the necessity of reprocessing the coated fuel particles to extract and recycle the TRU, we have identified the reprocessing system that could be used if it is necessary to reprocess the burned coated TRU fuel particles. The same processes discussed above, plus an aqueous process for separating the fuel matrix materials from the coated particles, would be employed.

III.F. Fuel Cycle

An emphasis in this investigation is achieving sufficiently high (>90% FIMA) TRU burnup that the coated fuel particles can be burned and then removed from the reactor and directly deposited in a waste repository without the necessity of reprocessing. To this end, we examined

a multibatch fuel cycle in which the reactivity decrease [from $k = 0.95$ at beginning of cycle (BOC)] associated with fuel burnup was partially offset by an increase in neutron source strength over the burn cycle. We estimate that control rod withdrawal could provide $\Delta k \leq 0.05$ but did not take this into account in the calculations.

Equilibrium fuel cycle calculations were performed with the REBUS fuel cycle code[17] using a two-dimensional (2-D), 33-group, S_8 neutron flux calculation. For the reference five-batch, 600-day burn cycle, 8.2-yr fuel cycle, the BOC TRU loading was 36 tonnes for the TRISO fuel and 47 tonnes for the BISO fuel. For both fuels, the BOC $k_{eff} = 0.95$ and neutron source $P_{fusion} \approx 40$ MW, and the EOC $k_{eff} \approx 0.81$ (0.87 for BISO) and neutron source $P_{fusion} \approx 170$ MW (107 MW for BISO). About 23% of the BOC TRU loading is fissioned in an 8.2-yr fuel cycle. The fuel would have to be resident in the core for about ten such fuel cycles to achieve 90% TRU burnup.

The GCFTR core is designed to operate at a nominal fission power level of 3000 MW(thermal), which corresponds to the fission of 1.1 tonnes/full-power year (FPY) of TRU. A typical 1000-MW(electric) LWR produces 0.36 tonnes/FPY of TRU. Hence, one GCFTR would be able to "support" (burn the TRU discharged from) three 1000-MW(electric) LWRs.

III.G. Depressurization Analysis

The fuel temperature rise following a depressurization loss-of-coolant accident (LOCA) was calculated. The decay heat following shutdown after 1 yr of operation was calculated with the ORIGEN code.[5] This heat source was used in a fuel pin temperature calculation with only a radiation cooling term (no convective or conductive cooling) and with the assumption that a fraction of the radiated power was reabsorbed in surrounding fuel pins. The fuel pin temperature increased up to an almost-saturated value of 1863°C at 48 h, for 50% reabsorption of the radiated energy, and 1942°C for 75% reabsorption of radiated energy. By comparison, the lowest TRU-oxide melting temperature is 2085°C (for Pu_2O_3), and the Zircaloy clad and matrix melting temperature is 1845°C. Thus, it appears that with some refinements to the design, the GCFTR could be passively safe with respect to the depressurization LOCA.

III.H. Electrical Performance Analysis

Using a Brayton cycle with 32% thermal-to-electrical energy conversion efficiency to convert the 3000-MW thermal power, the gross electric power production of a GCFTR would be 1024 MW(electric). The electrical power requirements for the operation of the GCFTR are 305 MW(electric), leading to an electric power amplification factor of $Q_e = 1024/305 = 3.4$ and a net electric power production of 719 MW(electric). The performance parameters are summarized in Table II.

TABLE II

Performance Parameters of GCFTR

Parameter	Value
TRU burnup	>90% FIMA
TRU transmutation rate	1100 kg/FPY
SNF transmutation rate	99.3 tonne U/FPY
LWR support ratio	3 GW(electric)
Fission thermal power	3000 MW(thermal)
Gross electrical power	1024 MW(electric)
Net electric power	719 MW(electric)
Electrical power amplification, Q_e	3.4

IV. FUEL DESIGN

IV.A. TRISO/BISO Fuel Particles

The TRISO/BISO coated fuel particle provides microscopic containment for the fuel and its FPs. Relative to traditional fuel used in fission reactors, it has the advantage of an additional level of FP containment, which may allow attainment of high fuel burnup and then burial without further reprocessing. We have examined the two coated fuel particles shown in Fig. 2.

The center region of the particle is referred to as the kernel and consists of the fissionable fuel, in our case TRUs. Immediately outside the fuel region is the buffer region, which is usually porous (50%) to allow for diffusion of fission gases and recoil of FPs. It can have an oxygen getter for decreasing free oxygen when the fuel is transmuted. This region is designed with greater than a 1-to-1 atom ratio of the Zr atom to each oxygen atom, which precludes CO buildup since ZrC has a higher oxygen potential in the temperature range (1400 to 1600 K) (Ref. 18). This region also should have 3.5 times as much volume as the fuel kernel to allow for recoil of fission by-products as neutrons interact with the fuel region. The next region is the inner pyrolytic carbon layer (IPyC). This region is primarily used to protect the fuel kernel from chlorine attack during the coating process but also provides structural support and acts as a first level of containment for the fuel. The next region consists of the third material, either ZrC or SiC in this study, which provides structural support and under irradiation will shrink to provide an inward pressure to counteract the outward pressure from the buffer and fuel regions. For the TRISO particle, there is an additional outer pyrolytic carbon layer (OPyC) primarily to prevent the SiC layer from interacting with cladding materials.

In thermal reactors, TRISO particles are usually embedded within a carbon matrix and burned in a thermal spectrum. The GCFTR may require a metal matrix to achieve a faster neutron spectrum, which in turn would necessitate an outer layer compatible with a metal matrix

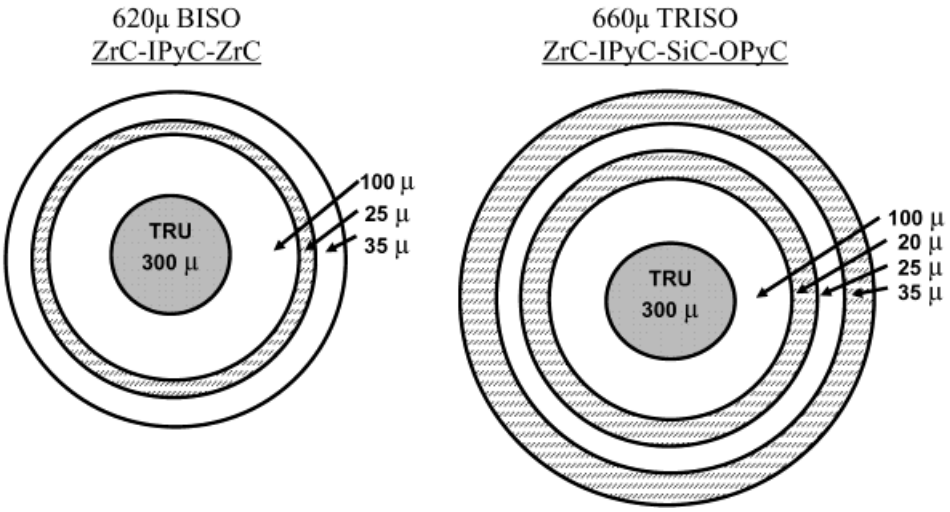

Fig. 2. BISO and TRISO coated fuel particles.

such as Zircaloy. For compatibility with such a matrix, the BISO outer layer was chosen to be ZrC.

If the current inventory of SNF from LWRs is processed using TRUEX and UREX, 99.995% of uranium and 100% of the lesser actinides are removed. The representative TRU composition[19] used in this paper is summarized in Table III. Because of the relatively low melting points of the elements in Table III, they would be formed into oxides with the melting temperatures given in Table III.

Use of carbides and nitrides[20] is also a possibility. The processing of TRU carbides proves problematic in the case of americium, however, because it vaporizes at typical ceramic processing temperatures.[18] Carbide kernels are also undesirable because they tend to fail because of FP damage to the SiC layer. On the other hand, were the kernel composed purely of TRU oxides, failure would tend to occur because of kernel migration and $CO_{(g)}$ pressure. Homan et al.[21] suggest that for a uranium fuel, an oxy-carbide mixture would minimize the failure modes of both oxides and carbides if the carbide-oxide ratio were between 15/85 and 50/50, with 35/65 being optimal. Lindemer[18] indicates that these ratios also can be applied to plutonium kernels. The TRU kernel is ~85% plutonium by mass (Table III), suggesting that forming an oxy-carbide TRU kernel in the appropriate ratio would obviate $CO_{(g)}$ pressure and migration. However, the production of such an oxy-carbide kernel is complicated by the aforementioned americium volatility. Carbonizing a fraction of the plutonium only in lieu of carbonizing a portion of each TRU mixture entails agglomeration, which cannot be assured to consistently attain the appropriate ratio, nor form as a microsphere.[22]

Thus, the only known feasible method appears to be to use the oxide form and resolve the problems inherent to that form. Carbon monoxide gas pressure is caused by a surplus of oxygen freed by fissioning of the TRU oxides, which in turn combine with the carbon of the buffer region. An oxygen getter would chemically combine with the oxygen and prevent it from forming $CO_{(g)}$. Even with an oxy-carbide mix, preliminary research showed "free oxygen" would cause a significant increase in pressure at high temperature (>1400 K). Additionally, a compact of some sort that helps maintain an inward pressure to counteract the outward pressure over a longer burnup period should help minimize fuel failure. Oxygen has a greater affinity for Zr than C through the reaction $ZrC + O_2 \rightarrow ZrO_2 + C$. Examining the oxygen potential diagram shows that oxygen prefers Zr over C at higher temperatures where ZrO stabilizes the freed oxygen atoms from the TRU fuel after it is fissioned. This not only lowers the free oxygen available to form $CO_{(g)}$, but also may preclude kernel migration thought to occur as CO dissociates at hot spots and recombines at colder spots around the kernel.[6] Thus, the use of porous ZrC as a buffer in lieu of carbon can compensate for an inappropriate carbon-to-oxygen ratio inherent in an oxide.

TABLE III

TRU Composition

Element	Mass Percent	Oxide	Melting Point (°C)
U	0.43	UO_2	2820
Np	4.32	Np_2O_3	2510
Pu	84.91	Pu_2O_3	2085
Am	10.21	Am_2O_3	2190
Cm	0.13	Cm_2O_3	2225

Pressure analysis was conducted using the ideal gas law and ORIGEN code[5] results for FPs from 97% burnup of TRU fuel. Pressure in the fuel particle versus burnup is shown in Fig. 3. The pressure from free oxygen increased almost exponentially. This would explain the Japan Atomic Energy Research Institute's increased particle failure rates with higher temperatures (1100 to 1300°C) but lower fluxes.[23] The pressure due to FP gases was negligible and easily contained within the void region of the buffer. However, the freed oxygen in the kernel that formed CO accounted for almost 75% of the total pressure, indicating the need for an oxygen getter. Ideally, sufficient room for expansion is obtained by ensuring that the buffer region void volume is 3.5 times the kernel volume.[18] For the TRISO and BISO with an oxygen getter (ZrC) in the buffer region, a void region of 1.8 times the kernel volume was decided upon because of reactivity constraints. This choice places a limit on the pressure and, consequently, a limit on the operating temperature for a given burnup.

For both TRISO and BISO models, higher temperatures create additional FP gases, Cs and Pd, which not only increase pressure but also may result in gases like Pd reacting with the TRISO SiC layer at high temperatures (>1830 K). Ideally, temperatures below 550°C are desired to control gas pressure. At lower temperatures ZrC and SiC have similar structural properties, whereas ZrC proved to be more resilient at higher temperatures.[24] If the outward pressure from gases is greater than the inward tensile strength, a rupture of one of the layers can result. If the outer shell also fails, this is called a "catastrophic failure," and FPs can escape. However, a secondary containment system can be used to capture or filter out FPs, i.e., a He extraction process. Redundancy for containment is already built into the particle's design.

It is our objective to achieve very high burnup without losing FP gas containment or structural integrity of the coated fuel particle. The GCFTR upper pressure limits on the BISO and TRISO are 352- and 345-MPa tensile strengths, respectively. This corresponds to an operational limit of 1700°C at 90% FIMA or 1520°C at 99% FIMA on the BISO, and 1690°C at 90% FIMA or 1510°C at 99% FIMA on the TRISO. To ensure that all layers maintain their respective structural integrity, the pressure should be limited to <200 MPa, which is the tensile strength limit of the pyrolytic carbon layer. Based on FP and $CO_{(g)}$ buildup, the TRISO and BISO particles are predicted to reach a conservative 160 MPa at 90% FIMA and 180 MPa at 99% FIMA for the GCFTR reference maximum fuel centerline temperature of 620°C (620°C allows for a power peaking factor of 1.2 relative to the fuel centerline temperature of 560°C discussed in Sec. V.B).

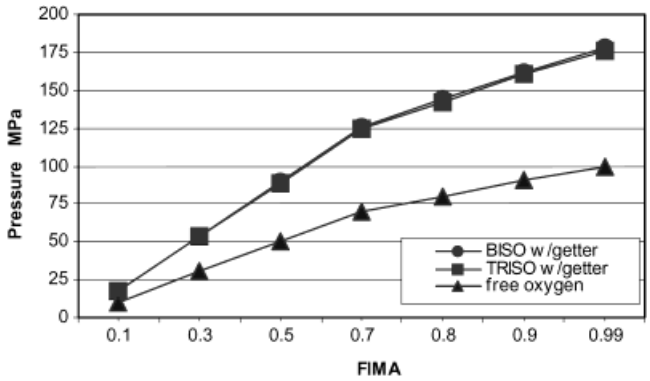

Fig. 3. Pressure buildup versus FIMA at operating temperature of 620°C.

IV.B. Radiation Damage Life

There are some data on irradiation of TRISO and BISO particles. Examination of the particles irradiated in the Peach Bottom reactor at temperatures of 1200 to 1400 K to a fast (>0.18-MeV) neutron fluence of 1.3×10^{25} n/m^2 found a failure rate of 1.4×10^{-6} (Ref. 25). More recent results[6] from coated particle fuel development programs in the United States and Germany have achieved burnups as large as 80% FIMA and fast neutron fluences as large as 1.2×10^{26} n/m^2 at irradiation temperatures of 800 to 1350°C. End of cycle release-to-production-rate ratios of the FP ^{85m}Kr varied from $O(10^{-4})$ to $O(10^{-6})$ for the higher FIMA U.S. experiments but were $O(10^{-7})$ to $O(10^{-9})$ for the O(10% FIMA) German experiments. By comparison, it is our objective to irradiate the TRU coated particle fuel in the GCFTR to 90 to 99% FIMA, corresponding to fast neutron fluences of 1.5×10^{26} and 2.9×10^{26} n/cm^2.

The GCFTR objective is to achieve burnup of 90 to 99% FIMA in fuel particles that retain sufficient containment capability that they can be deposited directly in a waste repository. The GCFTR will operate at a nominal total neutron flux of 5×10^{14} n/cm^2·s and fast (>0.1 MeV) neutron flux of 2×10^{14} n/cm^2·s.

Radiation damage to the matrix and clad materials is discussed in Sec. V.C.

V. CORE DESIGN

V.A. Nuclear Analysis

V.A.1. Effect of Fuel Choice on Transmutation and Radiation Damage Rates

In order to achieve high burnup without the necessity of reprocessing the coated fuel particle because of radiation damage, it is necessary to maximize the ratio of the TRU fission rate to the neutron damage rate. Since the capture-to-fission ratio for the TRU nuclides generally decreases with increasing neutron energy, utilization of

the neutrons to fission TRUs is improved by using a harder spectrum, in general.

As discussed in Sec. IV.A, two coated TRU fuel particle options are being considered: (a) a TRISO fuel particle with a ZrC buffer layer, pyrolytic graphite and SiC coating layers, and SiC matrix material and (b) a BISO fuel particle with the SiC coating layer replaced by a ZrC layer, the outer pyrolytic graphite layer eliminated, and SiC replaced by Zircaloy as the matrix material in order to achieve a harder neutron spectrum. The difference in neutron utilization of these two fuel options was compared by calculating the ratio of the TRU fission rate to the neutron flux >0.1 MeV (the latter of which was taken as a measure of the damage rate) for comparable cores based on the two fuel options [both with fuel volume percent 60%, He volume percent 30% and structural (ferritic steel) volume percent 10%]. The enrichment—ratio of the volume percent of the coated fuel particles to the volume percent of the "fuel" (coated particles plus matrix)—was 50%. The volume percent of the coated fuel particle occupied by the TRU kernel was 11.33% for the BISO and 9.39% for the TRISO. The TRU composition is indicated in Table III and given isotopically in Ref. 19.

Figure 4 shows the flux distributions of both the TRISO and BISO fuel configurations with similar $k_{eff} \approx 1.0$ values. This comparison shows that the BISO fuel has a harder neutron spectrum than the TRISO fuel because of the greater parasitic absorption (more zirconium) in the BISO and the greater moderation (more carbon) in the TRISO.

The effect of the harder BISO spectrum was examined by comparing a neutron utilization index (NUI), defined as the ratio of the TRU fission rate to the neutron flux above 0.1 MeV (which is a measure of the damage rate). The ratio of the NUI indices of TRISO/BISO is 1.09, indicating that the TRISO fuel has an ~10% larger fission rate per unit damage rate than the BISO fuel. Contrary to initial expectation, the harder spectrum of the BISO fuel does not appear to result in a significantly better transmutation-to-damage performance (NUI) than the softer spectrum of the TRISO fuel. The problem with the BISO fuel is that the Zircaloy matrix material has an absorption cross section that is competitive with ^{239}Pu (53% of fresh TRU), which greatly increases the parasitic neutron capture relative to that for the SiC matrix material in the TRISO fuel.

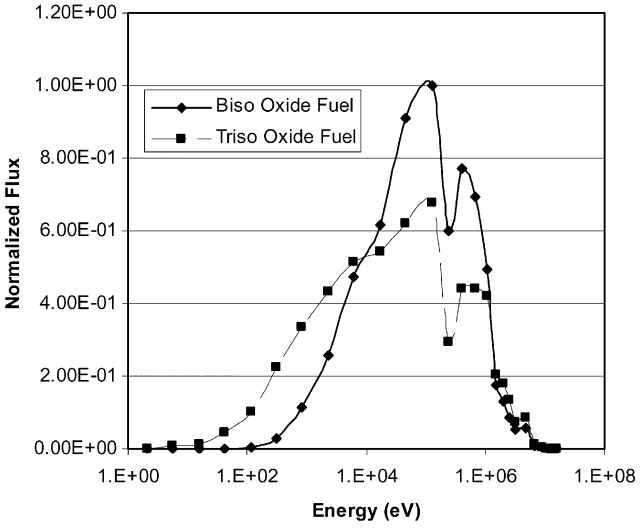

Fig. 4. Neutron spectra in the center of cores with BISO and TRISO fuel.

V.A.2. Effect of Enrichment and Core Thickness on k_{eff}

For the achievement of possible safety advantages, the maximum value of k_{eff} under normal operating conditions has been set to 0.95, as a trade-off between achieving a large neutron flux for transmutation and achieving a large reactivity margin to critical. The equilibrium loading of the reactor core fuel will be a combination of "burned" TRU fuel particles with reduced reactivity resulting from residence in the core during previous cycles and "fresh" TRU fuel particles. Taking into account this less reactive fuel and the possibility of the presence of control rods (that could be withdrawn over the burn cycle to compensate burnup reactivity), it was estimated that calculations with fresh TRU fuel should achieve $k_{eff} \approx 1.0$ if the same configuration with "equilibrium" TRU fuel is to achieve $k_{eff} \approx 0.95$.

Initial criticality calculations were made using both the BISO and the TRISO fuel configurations, first with an equal mixture of TRU oxide and TRU carbide, then with only TRU oxide. By varying enrichment (particle volume to particle plus matrix volume) of the fuel, the core fuel volume percentage, and the thickness of the core, the effect of the fuel type on the reactivity can be determined. The effect of enrichment on the neutron multiplication factor in a 1-m-thick core is shown in Table IV.

TABLE IV

Sensitivity of k_{eff} to Enrichment and Fuel Volume Percent

Fuel Type	Core Enrichment (%)	Core Fuel (%)	k_{eff}
BISO (oxide)	60	60	0.974
BISO (oxide)	60	65	1.016
BISO (oxide)	70	60	1.041
TRISO (oxide)	50	60	0.963
TRISO (oxide)	50	65	1.001
TRISO (oxide)	55	60	0.990
TRISO (oxide)	55	65	1.027

Recall that the fraction of the coated particle volume occupied by TRU differs between the TRISO (9.4%) and BISO (11.3%) particles.

Changing the enrichment of the fuel has a somewhat larger impact on k_{eff} with the BISO fuel than with the TRISO fuel since increasing the enrichment of the BISO fuel not only increases the TRU concentration but also reduces the Zr matrix concentration (reducing the parasitic absorption). Increasing the core fuel volume percent also has a somewhat larger effect with the BISO fuel than with the TRISO fuel.

To assess differences in the reactivity effect of leakage with the two fuels, the core thickness was varied. The results shown in Table V indicate the reactivity effect of leakage was about the same with the two fuel types.

As discussed above, the oxide fuel was selected over the mixed oxide (MOX)/carbide fuel because of fabrication and processing considerations. The above calculations indicate that the TRISO fuel is significantly more reactive than the BISO fuel because of the parasitic Zircaloy matrix material used with the latter, which causes us to tentatively identify a fresh fuel enrichment of 50% and core fuel volume percent of 60% for the TRISO fuel and an enrichment of 60% and a core fuel volume percent of 65% for the BISO fuel.

V.A.3. Benchmark Calculations

For benchmarking purposes, the Gem/Event[26] calculation used for the above analysis was compared with the TWODANT calculations.[27] The multiplication constant k_{eff} calculated by the EVENT code using the P_1 option and 30 group cross sections agreed to within $\Delta k = 0.007$ with the value calculated by TWODANT for the same model using the S_8 option and 33 group cross sections. A core model based on volume-weighted homogenization of the fuel particles, matrix material, structural material, and the helium coolant was used with both codes. A reflector composed of ferritic steel surrounds the entire core region. The GEM/EVENT code used 30 group cross sections processed[28] from the matxs10 library, while the TWODANT code used 33 group cross sections processed for a similar fast reactor composition from the ENDF-B/V cross-section library by the MC^2 code.[29]

As shown in Sec. IX, the enrichments considered above do in fact result in an equilibrium fuel composition with a BOC $k_{eff} \approx 0.95$, confirming the choice $k_{eff} \approx 1.0$ made for the above calculations with fresh TRU fuel.

TABLE V

Reactivity Effect of Leakage for BISO and TRISO Fuels

Fuel Type	Core Thickness (m)	k_{eff}
BISO (60 vol%, 65% enrichment)	0.9	0.967
BISO (60 vol%, 65% enrichment)	1.0	1.016
TRISO (55 vol%, 60% enrichment)	0.9	0.943
TRISO (55 vol%, 60% enrichment)	1.0	0.990
TRISO (55 vol%, 60% enrichment)	1.1	1.029

V.B. Thermal Analysis

The thermal design objectives for the GCFTR fission core were to have a thermal power generating capacity not to exceed 3000 MW, a specific power density not to exceed 50 W/cm^3, to use helium exclusively for all component and system cooling requirements, to achieve reasonable pumping requirements, to produce net electric power but not operate at temperatures so high that advanced material would be necessary, and to do all of this with technology that either exists or is being developed.

For the detailed thermal analysis of the reactor fuel and cooling, the configuration of the fuel was chosen as coated particles suspended in a matrix, which was then formed into clad fuel pins. Pins provide an additional barrier against FP release. Based upon the power density and the volume made available for the core, it was determined that approximately 207 200 pins distributed evenly throughout the core could be divided into five groups of 41 440 pins per zone to achieve the desired design objectives.

V.B.1. Axial Coolant Temperature Distribution

In order to perform the thermal analysis of the core, a few basic parameters were selected based upon typical pressurized water reactor (PWR) fuel pins as shown in Table VI. These parameters correspond to having the fuel occupy 65% of the core volume and the helium coolant occupying 25%, which leaves 10% for the structure.

The first step in evaluating the temperature distribution in the fuel pin was to determine the bulk coolant temperature. The governing relationship for this evaluation was the heat balance equation:

$$Q = \dot{m} C_p \Delta T \ ,$$

TABLE VI

Parameters Used for Fuel Pin Analysis

P/D Ratio	Clad Outer Radius (cm)	Clad Inner Radius (cm)	Gap Inner Radius (cm)	Pitch (cm)
1.06	0.67	0.61	0.60	1.417

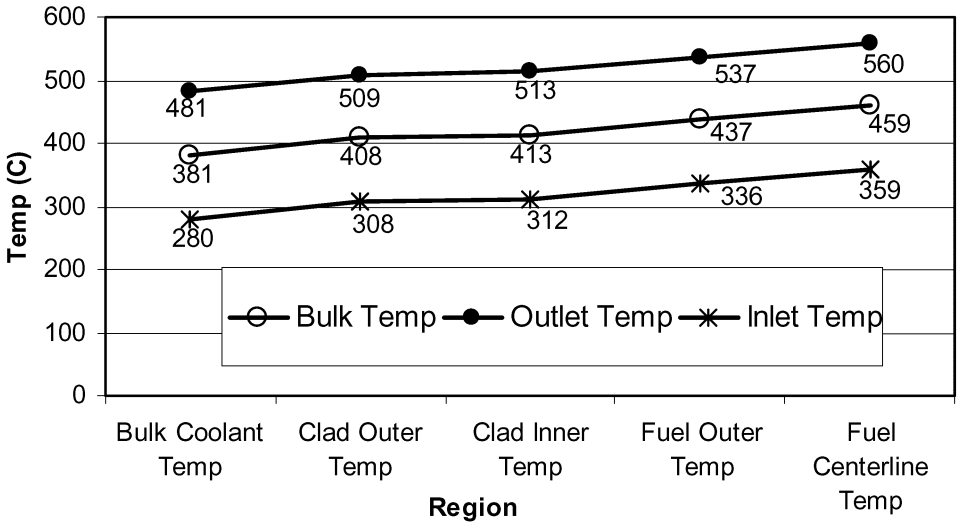

Fig. 5. Temperature distribution in the fuel pin.

where

Q = 3000 MW

C_p = heat capacity of He

ΔT = change in bulk temperature of the He coolant from the inlet to the outlet of the core.

A key parameter in the above calculations was the mass flow rate of the He coolant for the entire core and per coolant channel. The mass flow rate was first estimated by referencing the GT-MHR design[30] and scaling to the GCFTR parameters, then iteratively increased in order to optimize other operating parameters. For the ΔT of the coolant (Fig. 5), the mass flow rate of the core was optimized to be 2870 kg/s. The heat capacity of helium and other necessary properties were evaluated at the center bulk coolant temperature of ~380°C using the database of thermodynamic properties in the program "Engineering Equation Solver" (Table VII). Since the average bulk temperature was not initially known, the bulk coolant temperature and the property values of helium had to be evaluated iteratively, along with the mass flow rate.

In order to retain the option to use HT-9 clad, the maximum operating temperature of the coolant was limited to 500°C. The lower temperature of the coolant was dictated by the intent to investigate both the BISO particle with ZrC matrix and the TRISO particle with SiC matrix. Since graphite has a tendency to swell under irradiation at low temperatures, the lower (inlet) temperature of the fuel was set at 280°C at the entrance (or bottom) of the core. From the heat balance equation, the bulk coolant temperature at the outlet (top) of the core was found to be 481°C. The average bulk coolant temperature was assumed to be the arithmetic mean of entrance and exit temperatures, 381°C, and this value was assumed to be the midplane coolant temperature.

V.B.2. Radial Temperature Distribution in Fuel Pin

Once the bulk coolant temperature was known, a thermal resistance model[31,32] was used to determine the centerline temperature of the fuel at the three axial locations mentioned above. The fuel was assumed to be a homogeneous mixture of matrix, fuel kernel, and particle coating layers. This homogenous fuel was assumed to be encompassed by a layer of helium gap and then a layer of Zircaloy clad to create a fuel pin.

The thermal conductivities used in the above calculations are listed in Table VIII. The value of h for helium

TABLE VII

Coolant Properties

Pressure (MPa)	Average Temperature (°C)	Density (kg/m^3)	Viscosity (kg/m·s)	Thermal Conductivity (W/m·K)	Specific Heat (J/kg·K)
7	380	5.093	3.37×10^{-5}	0.26	5188

TABLE VIII

Thermal Properties of Fuel

Thermal Conductivities (W/m·C)	
κ_kernel	2.75
κ _PyC	3.5
κ _ZrC	20
κ _matrix	18.94
κ _fuel, homogenized	16.87
κ _gap (helium)	0.26
κ _clad	18.94
h (He coolant) (W/m^2·°C)	4161.81

was found by modifying the Nusselt number for a circular tube for coolant channel geometry. The Nusselt number is dependent on the Reynolds number and Prandtl number, which are also dependent on geometry and can be modified from the circular tube to coolant channel geometry.[31] The resulting temperature distributions within the fuel pin are plotted in Fig. 5.

The maximum temperature of the clad is 513°C, which is well below the melting temperature of 1845°C for Zircaloy. The maximum temperature in the fuel is 560°C. This temperature is well below any operating temperature limits of the TRU particle, but a more detailed calculation was performed in order to find the actual maximum temperature in the kernel of the TRU fuel particle.

V.B.3. Temperature in Fuel Particle

In order to determine the maximum temperature in the particle, a second thermal resistance analysis[31] across the layers of the particle was performed. The thermal resistance equations from the previous evaluation were modified for a spherical geometry, rather than a cylindrical one, with the appropriate thermal conductivities for the particle layers (Table VIII). Also, in the general pin analysis above, the homogenized fuel volumetric heat generation q''' (42.17 MW/m^3) was assumed to be uniform across the particle/matrix fuel element. For the single-particle analysis, a local heterogeneous value in the kernel of the fuel particle of q''' (63.05 MW/m^3) was found, assuming that heat was generated only in the fuel kernel and that the fuel kernels constituted 55% of the particle/matrix fuel (i.e., 55% enrichment). Because of the lack of sufficient data on TRU thermal properties, the thermal conductivity of the fuel kernel had to be estimated. Since the kernel contained ~85% Pu_2O_3, the thermal conductivity was assumed to be the same as $(U, Pu)O_2$ MOX fuel containing 85% PuO_2 at ~380°C (Ref. 31). Also, the thermal conductivity of the ZrC had to be corrected for 50% porosity in the buffer layer, which gives a value of 8 W/m·°C for that particle ZrC layer.

The particle was assumed to be at the fuel centerline, where the highest temperature would be. The three locations at the top, center, and bottom of the core were again evaluated. The temperature boundary condition at the surface of the particle was set equal to the respective peak temperatures of the above homogenized fuel calculations, or 560, 459, and 359°C. Since the thickness of the particle layers is <1 mm, the increase in temperature from the particle surface to the kernel center was only ~0.5°C.

V.B.4. Pressure Drop

The total number of coolant channels in the core was assumed to be the same as the number of pins. The initial approximation of the number of pins is conservative, but small variances in the number of pins do not seem to have a significant impact on the overall thermal analysis of the core. For the pressure drop calculations, 207 200 pins with an equivalent number of coolant channels was assumed, resulting in a mass flow rate per channel of 0.014 kg/s. Using thermohydraulic fundamental equations,[31] the results of Table IX were calculated. Several assumptions had to be made for these calculations. The number of spacers was established to be 8, typical for a PWR assembly. Also, the area of the entrance and exit plenums was assumed to be much larger than the area of the coolant channels in order to get the entrance/exit pressure drops.

Once the total pressure drop for one channel was known, the pumping power for the core could be calculated using the following equation:

$$Pumping\_Power = \frac{\dot{m}_{channel} \times \Delta P_{channel}}{\rho_{He} \times \varepsilon} \times number\ of\ channels\ ,$$

where ε is the pumping efficiency, assumed to be 85%. The resulting pumping power is 0.15 MW, only a small fraction of the power generated in the core.

V.C. Radiation Damage of Structure and Clad

In choosing the structural materials for the core design, there were two main considerations. First, although

TABLE IX

Core Coolant Pressure Drop

	Component				
	Friction	Spacers	Entrance/ Exit Plenums	Gravity	Total
Pressure drop per channel (kPa)	52	10.5	7.44	150	220

replacement of the structural materials is expected, the radiation damage limits should be high enough to avoid the necessity of frequent replacement. In addition, the material must be compatible with the system's thermal, chemical, and mechanical stress environment.

The potential structural materials chosen were ODS and HT-9 steel. Although the two steels share similar properties, ODS allows for a higher operating temperature of 650°C, ~100°C higher than the limit for HT-9 steel.[33] However, ODS, as a relatively new type of steel, lacks as complete a design database as some other materials. Comparatively, HT-9 steel has been more widely documented in its applications and limitations but also has a more constricted upper operating temperature limit. Because of the lack of a more extensive database for the ODS alloy, HT-9 steel was chosen as the reference structural material.

The radiation damage limit of HT-9 steel has been documented as 80 to 150 dpa, corresponding to a fast neutron fluence of $\sim 1.5 \times 10^{23}$ to 3×10^{23} n/cm^2 (Ref. 7). This corresponds to a lifetime of 23 to 48 EFPY [based on a core average fast ($E > 0.1$ MeV) flux of 2×10^{14} n/cm$^2 \cdot$s]. If the GCFTR operates for 40 yr at 75% availability (30 EFPY), the core structure may have to be replaced once.

Zircaloy-4 and HT-9 were identified as candidate clad materials. With HT-9 clad, the same radiation damage lifetime as discussed above would be expected. The higher temperature limits of Zircaloy make it an attractive candidate for the clad and, with the BISO fuel, the matrix material. Determination of the radiation lifetime of Zircaloy-4 is quite complex. Although growth phenomena and dislocations due to irradiation have been recorded at a fast neutron fluence of 5.8×10^{21} n/cm^2 (Ref. 34), the amount of annealing that takes place is great enough that Zircaloy maintains structural integrity and most of its good mechanical properties up to 20 dpa, corresponding to a fast neutron fluence of 10^{22} n/cm^2. This fluence would correspond to 3.2 EFPY in the GCFTR. However, this limit may be too conservative, since many commercial reactors operate with Zircaloy clad fuel for longer times.[35]

VI. REFLECTOR AND SHIELD DESIGN

The inboard shield shown in Fig. 1 is designed to protect the TFCs from radiation damage and to reduce nuclear heating to an acceptable level, i.e., resulting in a reasonable power required to cool the TFCs. The inboard reflector will reflect escaping neutrons back into the core, and the outboard shield/reflector combination is identical to the inboard. The superconducting magnets are considered lifetime components. The radiation damage limit to the insulators is 1×10^9 rads with currently available epoxy insulators and 1×10^{10} rads with more advanced ceramic insulators, while the Nb_3Sn superconductor has a fluence limit of 1×10^{19} fast neutrons/cm^2 (Ref. 8).

An MCNP model[9] was developed for the reflector and shield analysis. The shielding effectiveness of the reflector, shield, and vacuum vessel inboard of the plasma chamber and first wall was the primary emphasis of the investigation. The material composition for this region is given in Table X. HT-9 steel is a very good reflecting material but not a particularly good shield. A shield of tungsten and B_4C was chosen because it is very effective at stopping neutrons and gammas. The vacuum vessel was HT-9.

The geometry of the GCFTR was simplified for this Monte Carlo model. The TFC set was modeled as a continuous annular magnet, when in reality there are 16 discrete TF magnets (which become a continuous ring on the inboard side but are separated on the outboard). This model is considered conservative because if a neutron passes through the vacuum vessel, it will enter the magnet material, in the MCNP model. In reality, there are many magnets spaced around the vacuum vessel, and many neutrons that go through the vacuum vessel will not enter the magnet. The model also treats all geometries as circular instead of elongated, an assumption that should not greatly effect the results.

Two sets of tallies were collected from MCNP, the neutron flux in the magnets (neutrons per square centimeter per source neutron) and the energy deposited in the magnets (mega-electron-volts per gram) by both neutrons and gamma rays. For the fast neutron flux damage evaluation, all neutrons with an energy of 0.1 MeV or greater were counted.

The fast neutron flux, calculated on the basis of one plasma source neutron per second, can be converted into an actual neutron flux by multiplying by the actual emission rate of fusion neutrons and then used to calculate the fast neutron fluence by multiplication by the time of interest. For the energy deposition results, the conversion of 1 MeV/g to 1×10^{-8} rads is needed.[25] The tally obtained is multiplied by this conversion factor, the fusion power in neutrons per second, and by the time.

For protection of the magnets from neutron damage, an adequate thickness of the reflector plus shield plus 6-cm-thick vacuum vessel was found to be 79.5 cm. This includes a reflector with a thickness of 15 cm, a 61-cm-thick shield, and a 6-cm-thick HT-9 vacuum vessel.

TABLE X

Reflector and Shield Material Composition*

Region	HT-9	Helium Coolant	Tungsten	B_4C
Reflector	70	30		
Shield		20	40	40

*In volume percent.

An upper limit of the fast neutron fluence to the magnet can be obtained by assuming that the plant runs at the nominal fusion power of 180 MW and that the core k_{eff} is equal to 0.95 one hundred percent of the time. This assumption leads to a conservative estimate of the radiation damage to the magnets after 40 yr of operation at 75% availability that is slightly in excess of the superconductor fast neutron fluence limit, but to a radiation dose that has a comfortable margin of safety to the epoxy insulation limit.

Supercritical helium is used as the coolant for removal of the nuclear heating from the superconducting magnets. An ideal Carnot cycle operating between room temperature and 4 K would require 75 W of refrigeration power for every 1 W of heat removed from the magnets.[36] Assuming an efficiency of 50%, we use 150 W/W to determine the total amount of power necessary to cool the magnets. The magnet shielding results are summarized in Table XI.

VII. FUSION NEUTRON SOURCE

VII.A.1. Plasma Physics Analysis

VII.A.1. Design Constraints and Solution Methodology

To be consistent with our near-term physics and engineering philosophy, conservative ITER-like physics has been adopted for the design of the GCFTR tokamak neutron source. A reference normalized beta $\beta_N = 2.0\%$ is assumed, although operation at β_N values up to 2.5% is allowed for operational flexibility (β_N = plasma kinetic-to-magnetic pressure ratio $\div I/a\beta$).[10] A confinement multiplier $H = 1.0$ relative to the IPB98$(y,2)$ energy confinement scaling has been adopted.[37] The line average electron density is fixed at 75% of the Greenwald density limit to avoid confinement degradation at higher densities. An edge safety factor $q_{95} = 3$ is specified to avoid magnetohydrodynamic instabilities.

Standard aspect ratio–current (I_p-A) analysis[38] is employed to determine the major design parameters of the reference design. In this approach, the major geometric and operational parameters are expressed in terms of the aspect ratio A and plasma current I_p, taking into account the various physics and engineering constraints as well as the radial build constraint. The results of this calculation are shown in Fig. 6, where contours of major geometric and operational quantities (major radius R_0, fusion power P_{fus}, and fusion gain Q_p) are plotted in the I_p-A space. Solutions satisfying the radial build constraint, as determined by the flux core radius and thickness of the CS, the radial thickness of the TFCs, and the required thickness of the reflector and shield, must lie on the line labeled R_{in}. Based on the results shown in Fig. 6, an aspect ratio of 4, corresponding to a plasma current of 7.15 MA, was selected. The resulting major design parameters of the tokamak neutron source are listed in Table XII. This design choice provides us with a reference fusion power of ~180 MW, which meets the design requirements of the fusion neutron source. The choice of an aspect ratio $A = 4$ represents a reasonable trade-off between the need for low plasma current and large bootstrap current fraction, f_{BS} (and therefore reduced current drive requirements), while avoiding a drastic departure in aspect ratio range from the existing tokamak database.

TABLE XI

Magnet Shielding Results

Parameter	Value
Nominal fusion neutron source at 180 MW (n/s)	6.39×10^{19}
Nb_3Sn superconductor fast neutron fluence limit (n/cm^2)	1×10^{19}
100% availability of 40-yr fast neutron fluence (n/cm^2)	1.40×10^{19}
75% availability of 40-yr fast neutron fluence (n/cm^2)	1.05×10^{19}
Ceramic insulator radiation dose limit (rad)	1×10^{10}
Epoxy insulator radiation dose limit (rad)	1×10^{9}
100% availability 40-yr radiation dose (rad)	8.89×10^{8}
75% availability 40-yr radiation dose (rad)	6.67×10^{8}
Nuclear heating per magnet (kW)	8.67
Total nuclear heating in magnets (kW)	138.7
Power for cooling toroidal magnets (MW)	20.8

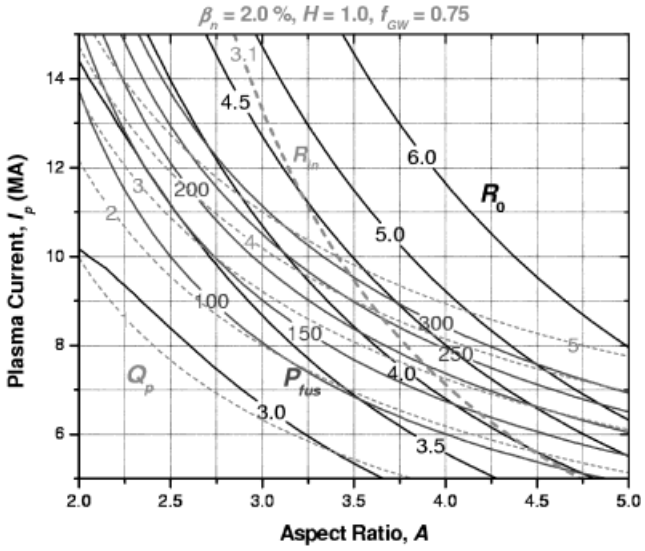

Fig. 6. The I_p-A contours of constant major radius.

TABLE XII

Major Plasma Design Parameters of the GCFTR Reactor

Parameter	Value
Major radius, R_0 (m)	4.15
Minor radius, a (m)	1.04
Aspect ratio, A	4
Plasma current, I_p (MA)	7.15
Fusion power, P_{fus} (MW)	181
Auxiliary power, P_{aux} (MW)	62.5
Fusion gain, $Q_p = P_{fus}/P_{aux}$	2.9
Neutron wall load (MW/m^2)	0.61
Magnetic field at R_0, B_0 (T)	6.29
$\langle n_e \rangle$ (10^{20} m^{-3})	1.53
$\langle T \rangle$ (keV)	7.4
Z_{eff}	1.38
Energy confinement time, τ_E (s)	0.84
Start-up (V·s)	82.5

VII.A.2. Operational Flexibility

To assess the operational flexibility of the tokamak neutron source based on the design parameters of Table XI, a plasma operational contour (POPCON) has been constructed and shown in Fig. 7. Contours of constant fusion power P_{fus}, normalized beta β_N, fusion gain Q, and ratio of exhaust to L-to-H-mode threshold power P/P_{thr} are plotted on a 2-D coordinate system with axes the volume average electron density $\langle n_e \rangle(y)$ and the density-weighted volume average plasma temperature $\langle T \rangle_n(x)$. The 100 and 75% Greenwald density limit boundaries are also shown.

The operating space is bounded on the left by the requirement $P/P_{thr} > 1$ to maintain H-mode confinement, on the top by the requirement that $n_e \leq 0.75 \times n_{GW}$, and on the right by the requirement that $\beta_N < 2.5\%$. This operating window provides sufficient flexibility to operate at fusion powers in the range to 50 to 200 MW, thus satisfying the BOC and EOC neutron source requirements for the GCFTR.

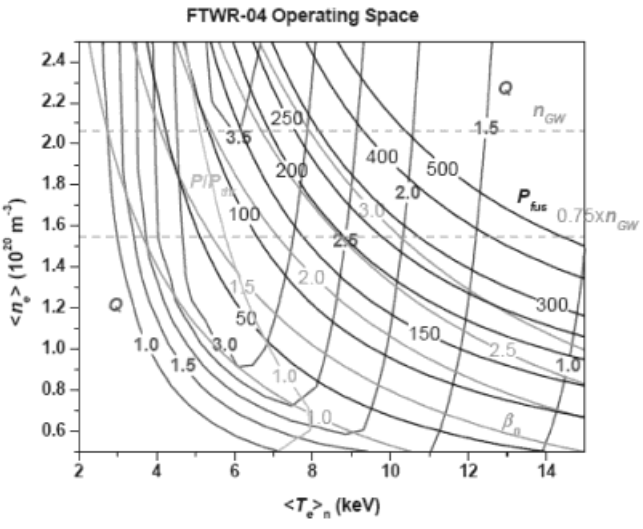

Fig. 7. POPCON for the GCFTR reference design parameters.

VII.A.3. Current Drive Considerations

The GCFTR design relies on steady-state operation of the tokamak neutron source. It is therefore important to demonstrate that such operation is feasible and consistent with conservative, near-term physics assumptions.

If f_{bs} is the bootstrap current fraction and if we do not take any credit for inductive burn contributions from the CS and the poloidal field (PF) coil (PFC) systems, the current that must be driven noninductively is equal to $I_{CD} = (1 - f_{bs})I_p$. Assuming that all auxiliary power $P_{aux} = P_{CD} = P_{fus}/Q_p$ is available for current drive and that the capabilities of the current drive system are described by the current drive figure-of-merit quantity $\gamma_{CD} = \bar{n}_{e20} R_0 I_{CD}/P_{CD}$ in units of 10^{20} m^{-2} A/W, the required current drive γ_{CD} is then equal to

$$\gamma_{CD} = \frac{\bar{n}_{e20} R_0 (1 - f_{bs}) I_p Q_p}{P_{fus}} \quad .$$

Our Fusion Reactor Design code has been run in constant fusion power mode ($P_{fus} = 200$ MW) to produce an aspect ratio scan and evaluate the required γ_{CD} for our design parameters using the above expression. A simple scaling[39] has been used for the calculation of the bootstrap current fraction:

$$f_{bs} = [1.32 - 0.235(q_{95}/q_0) + 0.0185(q_{95}/q_0)^2] \times \left(\sqrt{\frac{1}{A}} \beta_p \right)^{1.3} ,$$

where q_{95} and q_0 are the values of the safety factor at the edge and center, respectively, and β_p is the poloidal beta. The results of this simulation are shown in Fig. 8, where the bootstrap current fraction f_{bs} and the required current drive efficiency γ_{CD} are plotted against the aspect ratio.

It can be seen from Fig. 8 that for our aspect ratio ($A = 4$), we would need a current drive scheme with $\gamma_{CD} \approx 0.5$ in order to operate the GCFTR in steady state. For comparison, the highest current drive efficiencies achieved in existing experiments are in the range of 0.45 [Joint European Torus (JET) with ion cyclotron resonance frequency + lower hybrid] and 0.35 (JT-60 with lower hybrid current drive).[40] Therefore, the GCFTR current drive requirements are reasonable and consistent with the near-term physics and engineering database.

VII.B. Magnet Analysis

The GCFTR tokamak neutron source depends primarily on three magnet systems to establish the necessary

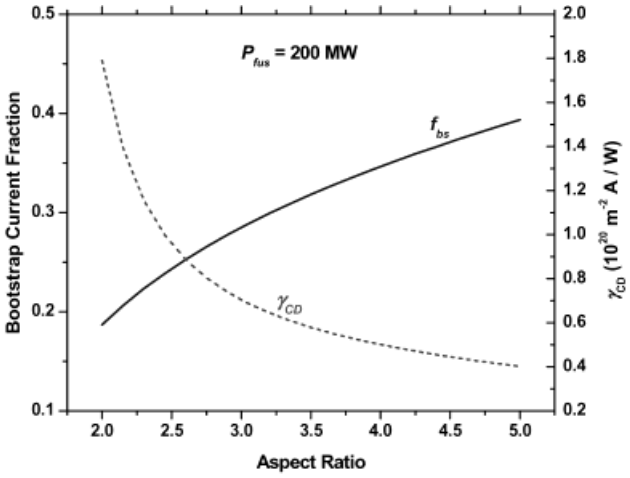

Fig. 8. Bootstrap current fraction f_{bs} and required current drive efficiency for the 200-MW reference GCFTR design.

fields in the plasma: the CS, the TFC, and the PFC systems. In this work, we focus only on the first two coil systems since they have a direct impact on the radial build of the tokamak reactor and, hence, on the overall size of the GCFTR.

VII.B.1. Central Solenoid

The CS is a vertically oriented solenoid that creates a changing magnetic flux that couples to the plasma and drives the start-up current as well as ohmically heating the plasma. The GCFTR CS is designed as an adaptation of the techniques and technologies developed for the ITER CS (Refs. 11, 12, and 13).

The conductor is composed of Nb_3Sn superconducting wire with copper stabilizer wound into cable. These cables are wound around a central liquid helium cooling channel. The assembly thus far is wrapped with a layer of insulator and surrounded by a thick structural jacket of Incoloy 908® and another layer of insulator. The Incoloy® jacket serves to handle the electromagnetic stresses created in the CS during operation. Incoloy® is used because it has a thermal expansion coefficient comparable to that of Nb_3Sn, thus removing the issue of thermal stresses. The detailed magnet conductor is indicated in Fig. 9.

The CS operates at high magnetic field in order to drive the greatest flux swing possible. The maximum (inboard) magnetic field at the beginning of operation is 13.5 T at 41.8 kA. Because of effects from the PFCs at end of burn (EOB), the maximum magnetic field is −12.8 T at 46 kA (Ref. 11).

The overall dimensions of the CS coil (flux core radius R_{fc} and radial thickness Δ_{OH}) are determined by the flux swing requirements, the geometry constraints imposed by our choice of ITER magnet technology, and the tensile stress limits.

The conductors are assembled into electrically independent blocks called "pancakes." These pancakes are then stacked vertically and reinforced structurally to form the CS. The radial thickness of the CS coil, Δ_{OH}, is determined by the number of radial turns needed to produce the 13.5-T magnetic field. Using the ITER design parameters and allowing for a small safety margin, it was found that 12 turns of ITER superconducting cable would meet

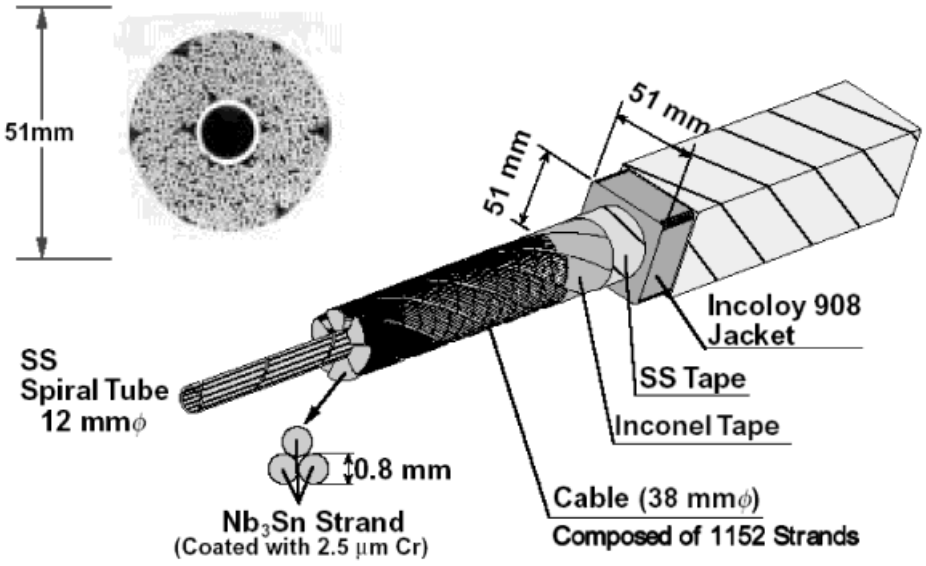

Fig. 9. Detailed cross section of CS conductor.[13]

our flux swing requirements. The corresponding radial thickness, taking into account insulation between turns and allowing for gaps, was found to be equal to 0.70 m while the flux core radius R_{fc} is equal to 0.66 m. This CS configuration produces 86.3 V·s, an amount sufficient to drive the 7.15 MA plasma current during start-up (see Table XIII). The CS coil design parameters are summarized in Table XIII.

VII.B.2. TF Magnets

The design of the TF magnet system is also adapted from the ITER design and technology[11,12] developed for ITER. The conductor is based on the ITER TF cable-in-conduit. It consists of Nb_3Sn superconducting cable (with Cu stabilizer) wrapped around a supercritical helium cooling channel, just like the CS conductor discussed earlier. The cable is then encased in a circular steel jacket for structural support. Although a detailed design of the winding pack configuration of the TFCs has not been carried out, it is envisioned to be similar to the ITER design where the conductors are arranged in radial plates. The GCFTR TFC design parameters are listed in Table XIV.

A detailed structural analysis of the TFCs is a difficult task, requiring the use of sophisticated finite element codes, and is beyond the scope of this scoping design study. However, simple scaling considerations can be employed to support the structural integrity of the GCFTR TFC system design: Since the GCFTR winding pack, TFC magnetic fields and currents, and TFC cross-sectional area are similar to ITER, while the major radius of the GCFTR coil is smaller, stresses and loads are expected to be smaller compared to ITER. Since GCFTR uses the same conductors and structural materials as ITER, its magnets should be able to meet the structural requirements.

TABLE XIII

CS Parameters

CS Conductor Parameters	
Superconductor	Nb_3Sn
Operating current (kA) IM/EOB[a]	41.8/46.0
Nominal B field (T) IM/EOB	12.4/13.5
Cable diameter (mm)	38.2
Conductor outer dimensions (mm)	51 × 51
Flux core radius, R_{fc} (m)	0.66
CS coil thickness, Δ_{OH} (m)	0.70
VS_{start} (V·s)	86.3
σ_{CS} (MPa) IM/EOB	194/230
σ_{max} (MPa) (ITER)	430
f_{struct}	0.564

[a]IM = initial magnetization.

TABLE XIV

TFC Parameters

Parameters	
Radial thickness, Δ_{TF} (m)	0.93
Number of TFCs, N_{TF}	16
Current per coil (MA), I_{TF}	8.16
Number of conductors per coil (turns), N_{cond}	120
Conductor diameter (mm), d_{TF}	43.4
Superconductor material	Nb_3Sn
I_{cond}, current per conductor (kA)	68
B_{max}, maximum magnetic field (T)	11.8
Radius of maximum field (m)	2.21
B_0, magnetic field on axis (T)	6.29

VII.C. Divertor and First-Wall Design

VII.C.1. Divertor

For the overall design of the divertor assembly, the ITER–Engineering Design Activity[14] (EDA) design is used as a starting point, and modifications are proposed here to adapt it to the GCFTR requirements. The material composition of the vertical targets and dome follow ITER explicitly in that the surface is lined with tungsten and backed with a layer of copper that bonds the surface tiles to a CuCrZr alloy matrix. The coolant channel and manifold will be constructed from this matrix material. The targets and dome are then mechanically fastened to a stainless steel cassette body just inside of the vacuum vessel wall shell.

The only necessary departure from the ITER design is related to the use of helium gas as a cooling medium instead of subcooled water. It should be noted that the cooling channel flow volume and surface area need to be significantly increased in order to accommodate the use of helium as a coolant because of the great difference in their respective specific volumes (water: 0.00104 m^3/kg; He gas: 0.3903 m^3/kg). By encasing the void space behind the vertical targets and dome to form a coolant manifold, and by adding a significant number of cooling fins from the non-plasma-facing surfaces, the effective flow area and coolant channel volume required can be achieved without significantly compromising the physical dimensions of the cassette and divertor structure. The planned layout of the divertor for helium cooling is illustrated in Fig. 10.

Using the base steady-state heat load and temperature data for the GCFTR, calculations were made for the necessary heat transfer surface area, coolant channel volume, and coolant velocity needed for a cooling system using helium gas. The computed GCFTR operating parameters for a fully loaded divertor and a half-power-loaded divertor are given in Table XV. The divertor heat loads come

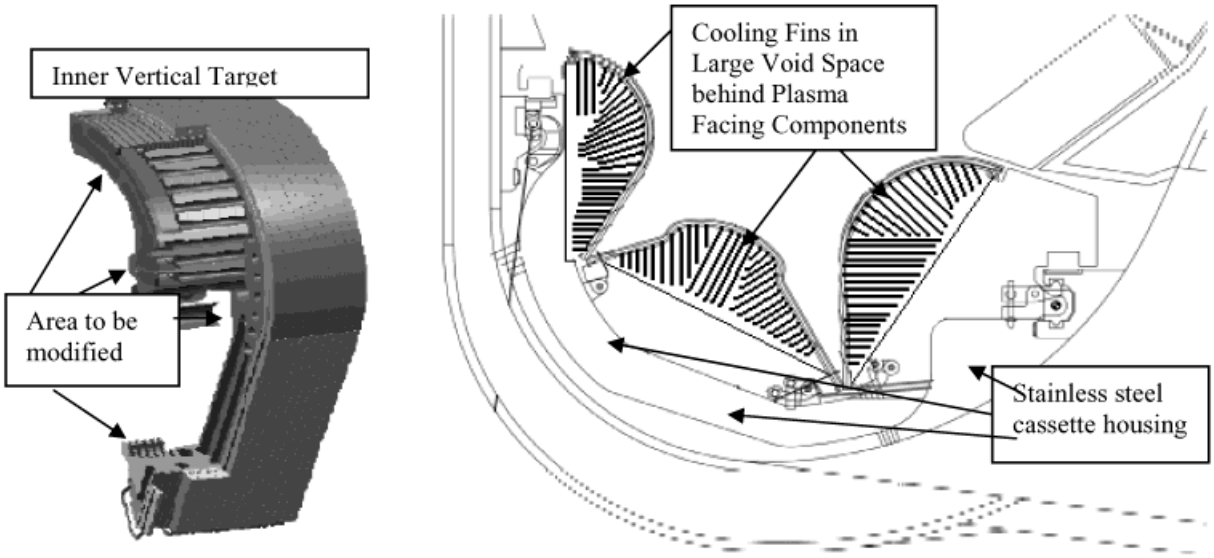

Fig. 10. Divertor assembly.[14]

from 20% of the 200 MW (maximum) fusion power that will come out of the plasma as heat. This exhaust heat will go either to the first wall as radiation or to the divertor. The full-load case assumes that all the heat goes to the divertor, and the half-load case assumes that only 50% of the heat goes to the divertor. The divertor design is capable of accommodating the full-load conditions.

A variable speed cooling system is used in order to vary mass flow rate as necessary in order to maintain the temperature rise across the assembly relatively constant at no greater than 50°C. The effective heat transfer surface area was estimated. Comparing properties of liquid water and helium gas at identical operating parameters and using the coolant mass and power balance equations, it was found that although helium and water have similar specific heat capacities (water: 4.213 kJ/kg·K; He gas: 5.191 kJ/kg·K), the velocity of helium gas would have to be two orders of magnitude greater than that of water in order to maintain the same temperature rise across the divertor assembly with the same coolant system configuration.

Since the poloidal plasma-facing elements are mounted onto a single steel support structure that incorporates toroidal cooling, the temperature difference within the structure must be limited to ~50°C, which provides a stable base for the plasma-facing elements. The impact of the materials thermal expansion would cause unacceptably high stresses if a temperature variance in excess of 50°C is permitted to occur. This requirement significantly increases the pressure drop across the divertor and the subsequent pumping power requirements. In order to keep the magnitude of the pumping power and pressure drop within reason, the cooling system for the divertor must be segmented into separate loops in order to keep the total pressure drop and pumping power per loop to within realistically achievable values. The corresponding pumping power requirement for the divertor under full-load conditions using helium gas coolant is 143.6 MW.

VII.C.2. First Wall

The purpose of the first wall in the GCFTR is primarily structural, but it also acts as a protective liner,

TABLE XV

GCFTR Divertor Operating Parameters

	Steady-State Surface Heat Loading (MW/m^2)	Total Heat Loading (MW)	Outer Surface Area (m^2)	Heat Transfer Effective Surface Area (m^2)	Coolant Temperature Rise (°C)	Coolant Mass Flow Rate (kg/s)	Coolant Velocity (m/s)	Coolant Pressure Drop (MPa)	Coolant Pumping Power (MW)
Full load	2	40	10	4	50	231.2	48	2.5	143.6
Half load	1	20	10	4	50	77.1	16	0.9	17.2

minimizing the introduction of contaminants into the plasma chamber. For the purposes of our design, the core wall that faces inward toward the plasma chamber will serve double duty as the outer radial surface of this structure. The core wall is made of HT-9 steel, and its radial inner surface facing the plasma chamber will be coated with beryllium 0.5 cm thick.

The upper, radial inner, and radial outer surfaces are similarly combined with the structure of the reflector assembly, as in the ITER-EDA design. For the upper and radial inner surfaces, the structural material of the first wall will consist of HT-9 steel, measuring 2 cm thick, and will have a surface coated with beryllium 0.5 cm thick. The core wall will receive the beryllium coating and serve as that portion of the system's first wall. The coolant channel configuration is a modified version of the ITER design in order to accommodate helium gas cooling. The full- and half-load data reflect that 20% of the 200-MW fusion power will come out of the plasma as heat. This waste heat will go either to the first wall as radiation or to the divertor. The full-load case assumes that all the heat is absorbed by the first wall, and the half-load case assumes that only 50% of the heat is absorbed by the first wall. The first-wall design is capable of accommodating the full-load conditions. The computed GCFTR operating parameters for a fully loaded and a half-power-loaded first wall are tabulated in Table XVI.

A variable speed cooling system is used in order to vary mass flow rate as necessary to maintain the temperature rise across the assembly relatively constant at no greater than 50°C for reasons similar to that of the divertor. The effective heat transfer surface area was estimated. Circular coolant channels will run within the centerline, between the beryllium layer and the back plate, in order to remove the heat deposited within the wall.

VII.D. Component Lifetimes

The operational lifetime of the first wall and divertor directly affect the availability of the GCTFR and influence its operational cycles. The first-wall design for this reactor is modeled after the ITER (EDA) first-wall design.[14] The structural material of the wall is HT-9, and it has a 0.5-cm sacrificial layer of beryllium on the side facing the plasma. The limiting factor will be the radiation damage to the HT-9, whose limit ranges between 80 and 150 dpa, corresponding to a fast neutron fluence of 1.5 to 3.0×10^{23} n/cm^2 (Ref. 7). Operation of the fusion reactor at 180 MW and at 75% availability for an estimated 40-yr life would correspond to a fast neutron fluence of 7.45×10^{23} n/cm^2. This result means that the first wall will need to be replaced two to five times during the life of the plant.

The most frequent operation to be performed is expected to be the replacement of the divertor because of erosion and damage. At steady-state operation and full heat loading, the divertor will sustain 2 MW/m^2 at the surface, less than the nominal value of 5 MW/m^2 for ITER, and will be exposed to a fast neutron fluence of $\sim 5.8 \times 10^{23}$ n/cm^2 over the life of the plant. For the ITER design, the replacement of the divertor is expected to be required eight times during the machine lifetime[41] because of erosion. We anticipate that erosion will also determine the divertor replacement rate in the GCFTR and expect that several replacements will be required over the lifetime of the GCFTR.

VIII. FUEL PROCESSING AND FABRICATION

The principal objective of the GCFTR is the transmutation of the LWR SNF. To do this efficiently, it is first necessary to separate the TRU from the uranium and FPs in the SNF. The TRU extraction involves UREX to extract the uranium followed by TRUEX to extract the FPs from the TRUs (Refs. 15 and 16). As discussed in Sec. IV, we plan to use an oxide of the resulting TRUs to make the kernels of the coated fuel particles. In addition, we are proposing some other options for future investigation, such as the plutonium extraction to form a TRU-O-C compound.

The processing of the LWR SNF is described schematically in Figs. 11 through 14. The overall reprocessing of SNF, fabrication of TRU fuel, and burn in GCFTR are indicated in Fig. 11.

The details of the SNF reprocessing are depicted in Fig. 12. The first reprocessing occurs in the UREX stage,

TABLE XVI

GCFTR First-Wall Operating Parameters

	Steady-State Surface Heat Loading (MW/m^2)	Total Heat Loading (MW)	Outer Surface Area (m^2)	Heat Transfer Effective Surface Area (m^2)	Coolant Temperature Rise (°C)	Coolant Mass Flow Rate (kg/s)	Coolant Velocity (m/s)	Coolant Pressure Drop (MPa)	Coolant Pumping Power (MW)
Full load	0.23	40	236.9	42	50	152.7	0.9	0.075	4.3
Half load	0.11	20	236.9	42	50	76.3	0.45	0.03	0.5

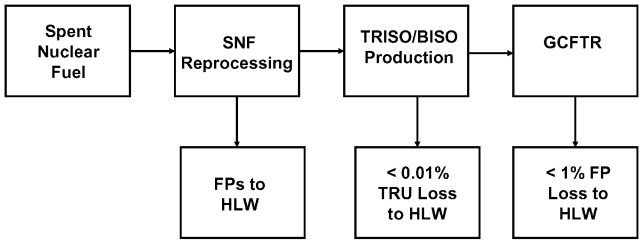

Fig. 11. GCFTR fuel cycle.

where 99.995% of the uranium is extracted and sent to be used for fuel in future LWRs. Next, the remaining 0.005% uranium, in addition to the FPs and the TRUs, is sent into a modified TRUEX stage, where the FPs are extracted and where the modification involves a trivalent actinide/lanthanide separation using a neutral extractant that is compatible with UREX and TRUEX. The remaining elements from the SNF, namely, 0.005% uranium and the TRUs, are sent to begin the TRU-oxide particle fabrication, resulting in <0.1% TRU loss. Finally, the TRISO/BISO fuel is sent to the GCFTR.

The TRISO/BISO fabrication flow diagrams are outlined in Figs. 13 and 14. Though the details vary between TRISO and BISO processing, the overall process is the same. Figure 13 shows the BISO production flow chart, and Fig. 14 shows the TRISO fabrication process. The 0.005% U and TRUs enter the fuel fabrication flow stream from reprocessing. They enter an evaporator, or in the Pu extraction case, the Pu is separated out by PUREX and then carbonized separately from the other TRUs. Those TRUs that enter the evaporator are sent to the calcine (where they are oxidized) and then to kernel blending and homogenization; if Pu were extracted, it would be reblended at this stage. Kernel homogenization gives the desired fuel blend necessary for maximum burnup. Then, the ZrC buffer, at 50% porosity, and the remaining layers would be coated onto the particles: two coatings for the BISO (IPyC and ZrC) and three coatings for the TRISO (IPyC, SiC, and OPyC).

As a result of the fuel we are utilizing, it is expected that the cladding will fail before the fuel (see Sec. V.C). It is important during the reprocessing of the fuel and cladding that the fuel particles are completely separated from the matrix material. There are numerous options for effective fuel-matrix separation using aqueous and dry matrix recycling. In addition, there is the option to recover ^{15}N for use as a nitride fuel.

IX. FUEL CYCLE ANALYSIS

IX.A. Methodology

The REBUS code[17] was used to analyze the GCFTR transmutation fuel cycle. REBUS performs a coupled 2-D neutron flux distribution (using the TWODANT discrete ordinates transport code[27]) and fuel depletion calculation and has many search options for iterative calculations. Enrichment searches were performed to determine the required ratio of TRISO/BISO particles to matrix material needed in order to achieve a given set of desired performance characteristics, in our case a BOC $k_{eff} \approx 0.95$, a fusion power limit of 200 MW, and a specified burn cycle length.

A five-batch fuel cycle, in which a given batch of fuel is resident in the GCFTR for five successive cycles, was modeled. A given batch of fuel was initially inserted into the outermost region of the core (region 1) for the first cycle and then moved to successively inward regions in successive cycles. This process continues until the fuel has been moved to the innermost region (region 5) of the core, resulting in a more even burn than if the fuel resided in any one region over the five-cycle residence time. Upon the completion of a five-cycle residence time, the fuel was removed, allowed to cool, and then mixed with fresh fuel and inserted back into region 1 or, if sufficiently burned, prepared for permanent storage. When the burned fuel is to be reinserted for another residence time, it will be separated from its matrix material and mixed with fresh fuel particles and then reconstituted in a new matrix and reinserted into region 1. Clearly, the fuel composition introduced into region 1 will change over time as once-burnt, twice-burnt, etc., fuel is mixed with fresh fuel until equilibrium is reached where the feed to region 1 is constant from cycle to cycle.

In the calculations performed for this study, there was an intermediate equilibrium in which fuel particles were modeled as passing through the reactor only once (i.e., particles were in the reactor only for one five-cycle residence time). At such an equilibrium, the fuel in the outermost region would be fresh, the next innermost region would be once-burnt, etc., and no mixing would occur after discharge from the innermost region. The results of such an intermediate equilibrium are a good approximation of the initial cycles of the first GCFTR. The fast spectrum of the GCFTR will not lead to a large shift in performance after multiple recycles, and these intermediate-equilibrium calculations can be used to project the result of continually recycling the fuel particles, as described above.

IX.B. Transmutation Performance

A number of transmutation fuel cycle calculations, as described above, were performed, corresponding to different choices of the core composition (fuel type, volume percent, enrichment; cycle length; etc.). The results of some of these calculations are shown in Table XVII.

Comparison of cases 1 and 3 or 2 and 4 shows that in order to achieve a comparable fuel cycle time and reactivity decrease (hence compensating increase in fusion power) over the fuel cycle, cores fueled with BISO fuel

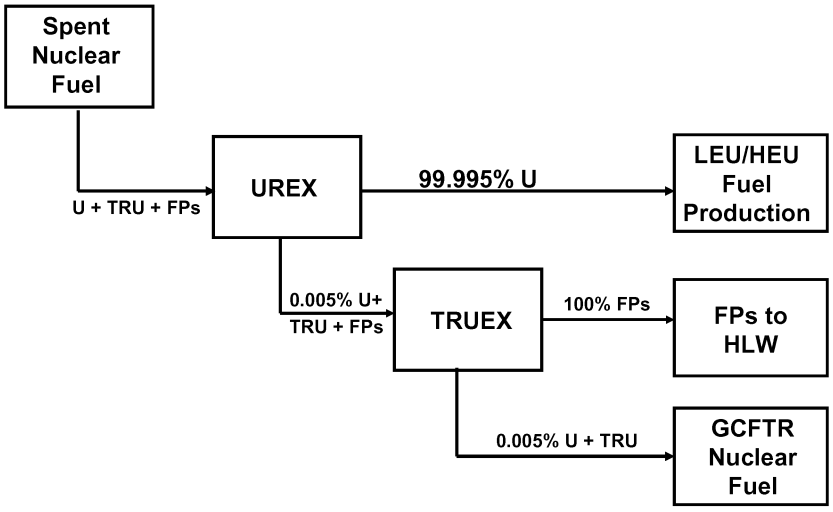

Fig. 12. SNF reprocessing.

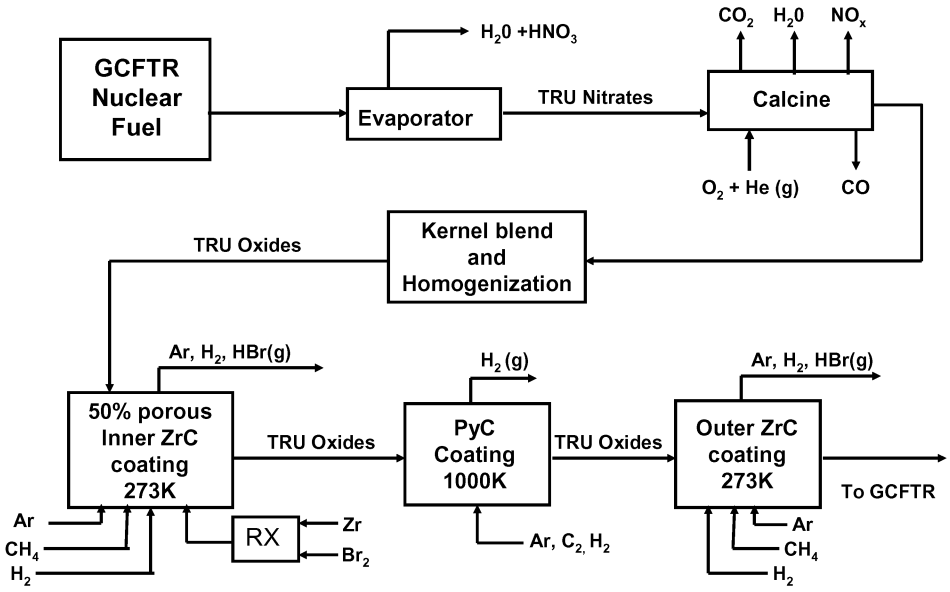

Fig. 13. BISO production.

particles/Zircaloy matrix must have a somewhat greater TRU loading than cores fueled with TRISO fuel particles/SiC matrix. The total residence time in the reactor required to achieve a given percentage TRU burnup, and hence the neutron fluence (and radiation damage), is somewhat greater for the BISO/Zircaloy fuel than for the TRISO/SiC fuel. These results arise principally from the greater parasitic absorption in zirconium than in SiC discussed in Sec. V.

Based on the calculations shown in Table XVII, the TRISO/SiC fuel with the 600-day burn cycle (case 1) was designated the reference fuel and fuel cycle for the GCFTR. The value of k_{eff} decreased over the fuel cycle (no account taken for compensating control rod movement) from ~0.95 at BOC to ~0.81 at EOC, and the fusion neutron source power increased from ~42 MW (BOC) to 172 MW (EOC) to maintain a constant 3000-MW(thermal) fission power over the cycle. The BOC TRU loading in the GCFTR is 36 tonnes, and 1.1 tonnes is fissioned per effective full power year. About 23% of the BOC TRU loading is fissioned in every 8.2-yr residence time. In terms of the original SNF from which the TRU was extracted, the disposal rate of the GCFTR is 99.3 tonnes/FPY.

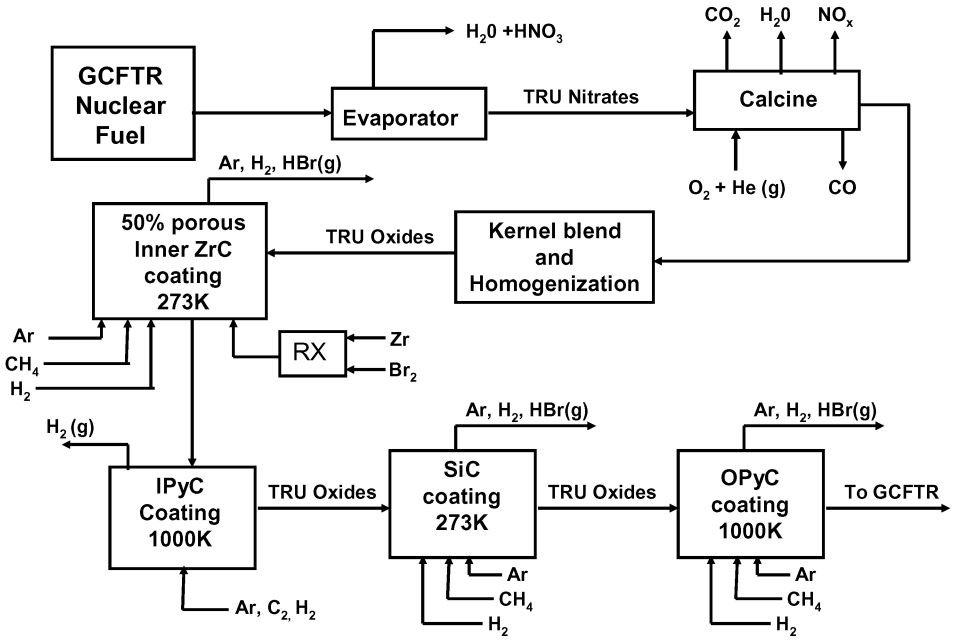

Fig. 14. TRISO production.

The above results can be extrapolated to calculate the total residence times (and the associated neutron fluences) in the GCFTR that would be required for the coated fuel particles to achieve 90 and 99% burnup. Eighty-years' residence in the GCFTR (about ten 8.2-yr fuel cycles) would be required to achieve 90% TRU burnup, and 159 yr's residence in the GCFTR (about nineteen 8.2-yr fuel cycles) would be required to achieve 99% TRU burnup. Based on the calculations shown in Table XVII, the TRISO/SiC fuel with the 600-day burn cycle (case 1) was designated the reference fuel and fuel cycle for the GCFTR.

Cases 2 and 4 are variants of cases 1 and 3, respectively, in which the burn cycle length is increased from 600 to 1000 full-power days. The TRU loadings are somewhat greater, the EOC k_{eff}'s are lower, and the EOC fusion powers and accumulated neutron fluences are higher for the 1000-day burn cycles, but otherwise, the characteristics of the 1000- and 600-day cycles are similar.

The GCFTR maintains a constant 3000 MW(thermal) of power as it transmutes LWR SNF. This corresponds to the destruction of 1.1 tonnes/FPY of TRU. Considering that a typical 1000-MW(electric) LWR produces TRU at a rate of 360 kg/FPY, one GCFTR can fission the TRU produced by three 1000-MW(electric) LWRs. The current capacity of the 105 LWRs in the United States is ~100 GW(electric), producing ~35.5 tonnes/FPY of TRU. It would therefore require a minimum of 32 GCFTRs at 100% availability (or 43 at 75% availability) to completely eliminate the annual TRU production in LWRs, at the present level of nuclear power in the United States.

X. DEPRESSURIZATION ANALYSIS

One of the design objectives of the GCFTR is that it meets the passive safety requirements of the GEN IV initiative.[1] Specifically, it must not depend on active engineered safety systems and must be able to maintain containment integrity during a design-basis depressurization LOCA. It must also contain all FPs within its design boundaries with no operator intervention for a period of 48 h. To examine the passive safety of the GCFTR, we have modeled a depressurization accident within the core. Such an accident would result in the reduction or elimination of the heat removal capability of the primary coolant system, causing a voiding of the coolant channels and virtual thermal isolation of the fuel pins. In LWRs, negative coolant voiding and fuel Doppler temperature coefficients of reactivity are important features in the early stages of such accidents. But, since our system has helium coolant and no ^{238}U, these temperature coefficients cannot be relied upon.

During the course of this accident scenario, the primary mode of heat transfer is eliminated, and the decay heat generated in the fuel is stored in the cladding, the matrix materials, the structural components, and the fuel particles themselves until the temperature becomes sufficiently large that radiative heat loss terms become important. In order to carry through a transient temperature analysis following depressurization, we made the simplifying assumption that the temperature of the cladding and fuel would quickly reach an equilibrium average value, allowing us to model the pin itself as a uniform temperature mixture with a net heat source

TABLE XVII

Transmutation Fuel Cycle Analysis for 3000-MW(thermal) GCFTR

Parameter	1	2	3	4
Fuel particle type	TRISO	TRISO	BISO	BISO
Kernel composition	TRU-O	TRU-O	TRU-O	TRU-O
Enrichment(particle/particle+matrix) (vol%)	62	76	60	65
TRU/core (vol%)	3.49	4.28	4.42	4.79
Matrix material	SiC	SiC	Zircaloy-4	Zircaloy-4
Burn cycles (batches)	5	5	5	5
Burn cycle length (days)	600	1000	600	1000
Five-cycle fuel residence time (yr)	8.21	13.69	8.21	13.69
BOC k_{eff}	0.946	0.950	0.953	0.954
EOC k_{eff}	0.809	0.755	0.873	0.807
BOC P_{fus} (MW)	42.1	38.8	36.7	35.5
EOC P_{fus} (MW)	172	236	107	175
TRU BOC load (tonne)	36.4	42.8	47.0	48.8
TRU burnup per year (tonne/FPY)	1.11	1.11	1.11	1.11
TRU burnup per cycle [tonne (%)]	1.8(4.6)	3.0(6.2)	1.8(3.6)	3.0(5.6)
TRU burnup per residence time [tonne (%)]	9.1(23)	15.2(31)	9.2(18)	15.2(28)
SNF disposed per year (tonne/FPY)	99.3	99.2	99.8	99.5
Average core flux across cycle (n/cm^2·s)	4.12E+14[a]	3.82E+14	4.09E+14	3.97E+14
Average core (>0.1 MeV) flux (n/cm^2·s)	1.63E+14	1.54E+14	1.67E+14	1.61E+14
Fluence/residence time (n/cm^2)	1.07E+23	1.65E+23	1.06E+23	1.71E+23
Fluence (>0.1 MeV)/residence time (n/cm^2)	4.23E+22	6.67E+22	4.33E+22	6.96E+22
Residence at 90% burn (yr)	80	99	103	110
Fluence at 90% burn (n/cm^2)	1.04E+24	1.19E+23	1.33E+24	1.38E+24
Fluence (>0.1 MeV) at 90% burn (n/cm^2)	4.12E+23	4.82E+23	5.42E+23	5.59E+23
Residence at 99% burn (yr)	159	197	205	219
Fluence at 99% burn (n/cm^2)	2.07E+24	2.38E+24	2.65E+24	2.74E+24
Fluence (>0.1 MeV) at 99% burn (n/cm^2)	8.18E+23	9.60E+23	1.08E+24	1.11E+24

[a]Read as 4.12×10^{14}.

$$Q_{net} = Q_{generated} - Q_{emissive} \ ,$$

where

$$Q_{emissive} = \varepsilon \sigma T^4 \times Area \ .$$

Since the heat generated by the fuel is coming only from the decay of FPs and actinides, the temperature in the core is strictly a function of time. The pin consists of 70% Zircaloy matrix and 30% BISO fuel particles (per unit volume) with an enrichment of 30%, and the pin's effective specific heat capacity was modeled accordingly:

$$C_p = 0.7(C_{p\text{-}matrix}) + 0.3(C_{p\text{-}fuel}) \ .$$

The initial average pin temperature for the calculation was 800°C, the total mass of the pin assembly was 1.711 kg, and the average specific heat capacity of the homogenized assembly was 196.11 kJ/kg·°C.

The decay heat following shutdown after 1 yr of operation was calculated with the ORIGEN code[5]; in units of kilowatts per tonne of fuel, the decay heating was 299 at $t = 0$, 167 at $t = 1$ min, 65 at $t = 1$ h, 9 at $t = 1$ day, and 8.3 at $t = 2$ days. The decay heat added by actinides is insignificant in magnitude when compared to that of FPs (thus not having a significant impact on temperature rise). Specifically, the initial decay heat produced by the FPs is 0.105 MW while the heat from the actinides is ~2 kW. Since FPs build up over core operating life, it is expected that the worst-case decay heat scenario will occur when four of the five fuel zones are composed of partially burned fuel. To simulate this situation, the ORIGEN decay heat was calculated after 1 yr of GCFTR operation.

The amount of radiated energy is largely dependent on the temperature of the structure (assumed to be a blackbody) and the emissivity ε, which is calculated as

$$\varepsilon = \frac{1 - \exp[-NTU(1 + Cr)]}{1 + Cr}$$

and

$$NTU = UA/C_{min} \ ,$$

where

Cr = specific heat ratio between the clad and fuel

NTU = number of transfer units

U = overall heat transfer coefficient

A = area of the pin

C_{min} = lowest specific heat value within the structure.

It is also important to take into account what is actually happening in the core in terms of emissive power. When heat is lost from a fuel pin due to thermal radiation, the heat is dissipated asymmetrically. Away from the inner and outer annuli of the reactor core, the heat being dissipated in the radial direction is offset by the fact that the adjacent pins will be receiving the heat and radiating comparable amounts of heat back to the focus pin, thus canceling out the $Q_{emissive}$ term in the radial direction. However, the reflector (and pressure vessel) receives heat from the pins located near the inner and outer radii, and there is a fraction of heat being radiated from both the top and bottom of each individual fuel assembly (the total fraction of core that actually emits heat by thermal radiation is estimated to be between 25 and 50%). Thus, an effective view factor—the fraction of radiated heat not reabsorbed—is used in the computation of the radiative heat loss term in our analysis. The decay heat values are initially 7% of the total core power density; i.e., for 50 W/cm^3 fuel region specific power density, the decay heat values have an initial value of ~3.5 W/cm^3.

The objective of the analysis is to determine when a material thermal limit will be reached, assuming no operator intervention. The thermal limits of the primary materials of construction are listed in Table XVIII. The calculated fuel pin temperature rise is tabulated in Table XIX.

These results indicate that the temperature rise in the core due to decay heat is significant enough during a design-basis depressurization LOCA that the matrix and cladding will reach temperatures that exceed their melting temperature 24 h after depressurization. Table XIX also illustrates that the temperature rise begins to stabilize between 24 and 48 h after shutdown. Thus, the design objective of passive safety with full containment has not yet been achieved under a worse-case scenario, but further analysis and some minor core configuration changes should allow the GCFTR to achieve the desired passive safety performance goal for the depressurization accident.

TABLE XVIII

Pin Material Critical Temperatures*

Zirconium Carbide	Pyrolytic Carbon	Zircaloy Cladding	Zircaloy Matrix	TRU-Oxide
3250	3650	1845	1845	2085

*In degrees Celsius.

XI. ELECTRICAL PERFORMANCE

The electrical performance goal of the GCFTR is that it be power self-sufficient under steady-state operating conditions. Any surplus power generation capacity can be routed to the commercial grid.

The use of helium as the coolant for all components and systems results in significant pumping power requirements. Because helium is the working fluid and will not undergo a phase change during the cycle, a Brayton power cycle will be used.

XI.A. Electrical Power Production

The maximum gross thermal power that the core will produce is 3000 MW. The ~200 MW of fusion power will not be directly converted into recoverable energy except through a feed preheat system that, by redirecting some of the fusion cooling waste heat back into the inlet stream of the core coolant system, will slightly increase the thermal efficiency of the core. The power cycle will be configured into four independent loops, each with a thermal power capacity of 750 MW. Each loop will correspond to a 90-deg arc section of the core containing 51 800 fuel pins. The Brayton power cycle is illustrated in Fig. 15.

The gross thermal efficiency of the Brayton cycle when the feed preheater is incorporated into the system is ~32%. The gross electrical power generation capacity of the GCFTR is 1024 MW(electric).

XI.B. Operating Power Requirements

The pumping power requirements for each of these four helium coolant loops represents a significant portion of the operating power required for the system and is briefly discussed here. The pressure drop over the components of the system can be seen in Fig. 15 and is input into the thermodynamic pumping power relationship:

$$Pumping\ Power = \frac{\dot{m}_{loop} \times \Delta P_{loop}}{\rho_{He} \times \varepsilon} \times number\ of\ loops\ .$$

The other primary loads that are accounted for in this evaluation are the cooling and operating power requirements of the TF, CS, and PF magnetic coil systems; the cooling power requirements of the divertor, first wall, shield, and reflector systems; the pumping power requirements through the core and power cycle components

TABLE XIX

Fuel Pin Temperatures Following Depressurization*

	0	5 (min)	10 (min)	30 (min)	60 (min)	700 (min)	12 (h)	24 (h)	48 (h)
1yb[a] at 25% view factor	800	1154	1256	1584	1652	1820	1841	*1908*[a]	*1942*[b]
1yb at 50% view factor	800	1136	1230	1541	1602	1760	1775	1835	*1862*[b]

*In degrees Celsius.
[a]Fission products corresponding to 1-yr burnup.
[b]Exceeds Zircaloy clad and matrix melting temperature.

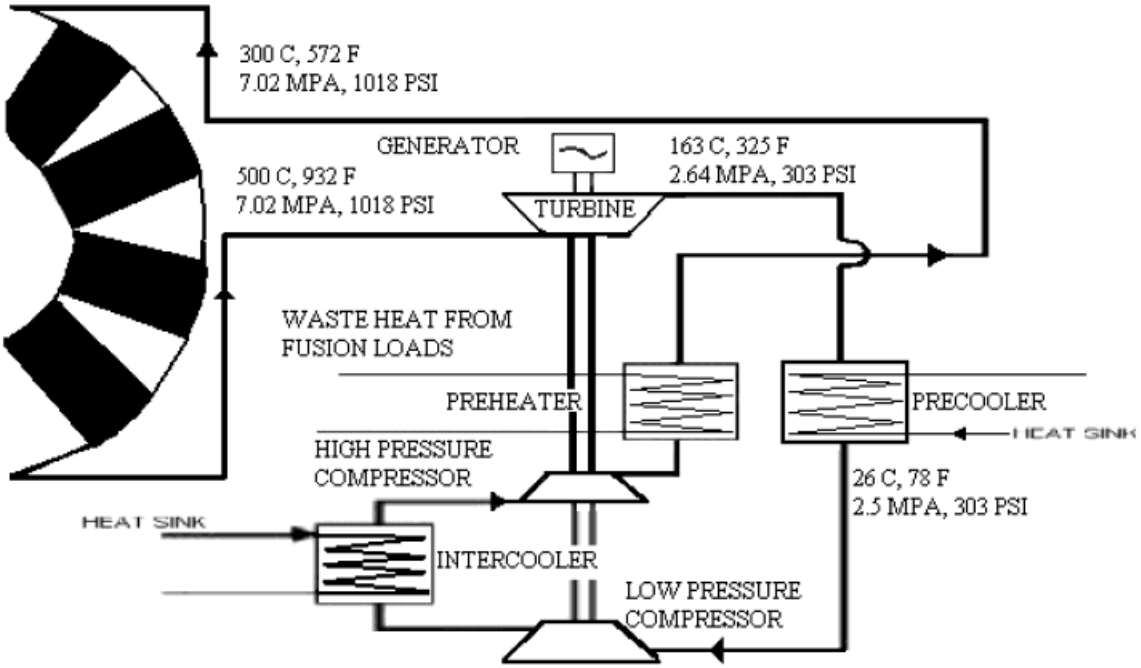

Fig. 15. One loop of the Brayton power cycle.

including turbines and heat exchangers; and the heating and current drive system requirements. The TFC cooling power requirement is discussed in Sec. VI, along with the first-wall, shield, and reflector cooling requirements. The CS and PFC cooling power requirements are estimated to be 1.2 MW. The divertor cooling requirement is derived in Sec. VII. The core pumping power requirements are derived in Sec. V. The heating and current drive system delivers 62.5 MW with an assumed efficiency of 70%, for a 90-MW requirement. The coolant system pumping power requirements were derived above. The calculated power consumption data are listed in Table XX.

XI.C. Net Electrical Power

By subtracting the total operating power requirement of 305 MW(electric) from the 1024 MW(electric) produced by the GCFTR, a net surplus power generating capacity of 719 MW(electric) is found. The electric power

TABLE XX

Power Consumption of Primary Loads*

Magnets	Heating and Current Drive System	Divertor Cooling	First Wall, Shield, Reflector Cooling	Core Cooling	Coolant System and Heat Exchangers	Total Operating Power Requirement
22[a]	90[a]	143[a]	3.9[a]	0.2	46	305

*In megawatts (electric).
[a]Approximately 10% of this waste heat will be recovered by using a feed preheater in the coolant system.

amplification factor for the entire plant is $Q_e = 1024/305 = 3.4$.

ACKNOWLEDGMENTS

The authors are grateful to S. Abdel-Khalik and N. Hertel for input on various aspects of this paper.

REFERENCES

1. "GEN IV International Forum: Nuclear Energy Systems for the Future," Web site ⟨http://gif.inel.gov/⟩.

2. "Advanced Fuel Cycle Initiative," Web site ⟨http://apt.lanl.gov⟩; see also ⟨http://www.nuclear.gov/afci⟩.

3. F. H. SOUTHWORTH et al., "The Next Generation Nuclear Plant (NGNP) Project," *Proc. Global 2003 Conf.*, New Orleans, Louisiana, November 16–20, 2003, American Nuclear Society (2003) (CD-ROM).

4. J-C. GARNIER et al., "Feasibility Study of an Advanced GFR," *Proc. Global 2003 Conf.*, New Orleans, Louisiana, November 16–20, 2003, American Nuclear Society (2003) (CD-ROM).

5. "SCALE: A Modular Code System for Performing Standardized Computer Analyses for Licensing Evaluation," NUREG/CR-0200, Rev. 5 (ORNL/NUREG/CSD-2/R5), Oak Ridge National Laboratory (1997).

6. D. A. PETTI, J. BUONGIORNO, J. T. MAKI, R. R. HOBBINS, and G. K. MILLER, "Key Differences in the Fabrication, Irradiation and High Temperature Accident Testing of U.S. and German TRISO-Coated Particle Fuel, and Their Implications on Fuel Performance," *Nucl. Eng. Des.*, **222**, 281 (2003).

7. B. B. KADOMTSEV, B. N. KOLBASOV, G. F. CHURAKOV, A. S. KUKUSHKIN, A. I. KOSTENKO, V. I. PISTUNOVICH, S. N. SADAKOV, G. E. SHATALOV, and D. V. SEREBRENNIKOV, "USSR-Contribution to the Phase IIA of the INTOR Workshop," Vol 2, p. VIII-64 (1982).

8. M. SAWAN, University of Wisconsin, Personal Communication (Feb. 2004).

9. X-5 MONTE CARLO TEAM, "MCNP—A General Monte Carlo N-Particle Transport Code," Version 5, LA-UR-03-1987, Los Alamos National Laboratory (2003).

10. ITER PHYSICS BASIS EDITORS, "Chapter 3: MHD Stability, Operational Limits and Disruptions," *Nucl. Fusion*, **35**, 2251 (1999).

11. ITER TECHNICAL BASIS, "Chapter 2.1: Magnets," G A0 FDR 1 01-07-13 R1.0 (2001).

12. M. HUGUET, "Key Engineering Features of the ITER-FEAT Magnet System and Implications for the R&D Programme," *Nucl. Fusion*, **41**, 1503 (2001).

13. H. TSUJI et al., "Progress of the ITER Central Solenoid Model Coil Programme," *Nucl. Fusion*, **41**, 645 (2001).

14. "Cost Review and Safety Analysis, International Thermonuclear Experimental Reactor Project Report," ITER Detailed Design Report (1996).

15. W. M. NUTT, R. N. HILL, and D. B. BULLEN, "Performance Assessment Modeling of High Level Nuclear Wasteforms from the Pyroprocess Fuel Cycle," Argonne National Laboratory (May 1995).

16. E. A. HOFFMAN, "Neutron Transmutation of Nuclear Waste," PhD Thesis, Georgia Institute of Technology (June 2002).

17. B. J. TOPPEL, "A User's Guide to the REBUS-3 Fuel Cycle Analysis Capability," ANL-83-2, Argonne National Laboratory (1983).

18. T. B. LINDEMER, "Thermochemical Analysis of Gas-Cooled Reactor Fuels Containing Am and Pu Oxides," ORNL/TM-2002/133, Oak Ridge National Laboratory (2002).

19. E. A. HOFFMAN and W. M. STACEY, "Comparative Fuel Cycle Analysis of Critical and Subcritical Fast Reactor Transmutation Systems," *Nucl. Technol.*, **144**, 83 (2003).

20. JAPAN ATOMIC ENERGY RESEARCH INSTITUTE, TOKAI LABORATORY, ACTINIDES SCIENCE RESEARCH GROUP, "JAERI's Success in Synthesis of Americium Nitride: For the More Efficient Transmutation of High-Level Radioactive Waste," *STA Today* (May 1999).

21. F. J. HOMAN, T. B. LINDEMER, E. L. LONG, Jr., T. N. TIEGS, and R. L. BEATTY, "Stoichiometric Effects on Performance of High-Temperature Gas-Cooled Reactor Fuels from the U-C-O System," *Nucl. Technol.*, **35**, 428 (1977).

22. T. B. LINDEMER, Oak Ridge National Laboratory (retired), Personal Communication (2004).

23. K. SAWA et al., "Prediction of Fuel Performance and Fission Gas Release Behavior During Normal Operation of the High Temperature Engineering Test Reactor by JAERI and FZJ Modeling Approach," *J. Nucl. Sci. Technol.*, **38.6**, 411 (June 2001).

24. K. MINIATO et al., "Irradiation Experiment on ZrC-Coated Fuel Particles for High-Temperature Gas-Cooled Reactors," *Nucl. Technol.*, **130**, 272 (2000).

25. E. LONG et al., "Fabrication of ORNL Fuel Irradiated in the Peachbottom Reactor and Postirradiation Examination of the Recycle Test Elements 7 and 4," Oak Ridge National Laboratory (Oct. 1974).

26. C. DE OLIVEIRA and A. GODDARD, "EVENT—A Multidimensional Finite Element-Spherical Harmonics Radiation Transport Code," *Proc. Int. Seminar 3-D Deterministic Radiation Transport Codes*, Paris, France, Organization for Economic Cooperation and Development (1996).

27. "DANTSYS: A Diffusion Accelerated Neutral Particle Transport Code System," LA-12969-M Manual UC-705, Los Alamos National Laboratory (1997).

28. R. E. MacFARLANE, "A Code for Interfacing MATXS Cross-Section Libraries to Nuclear Transport Codes for Fusion Systems Analysis," LA-9863-MS, Los Alamos National Laboratory (1984).

29. H. HENRYSON et al., "MC^2-2: A Code to Calculate Fast Neutron Spectra and Multigroup Cross Sections," ANL-8144, Argonne National Laboratory (1976).

30. M. P. LABAR, "The Gas Turbine—Modular Helium Reactor," GA-A23952, General Atomics (2002).

31. N. E. TODREAS and M. S. KAZIMI, *Nuclear Systems I: Thermal Hydraulic Fundamentals*, Taylor & Francis (1993).

32. F. P. INCROPERA and D. P. DEWITT, *Fundamentals of Heat and Mass Transfer*, John Wiley & Sons, New York (2002).

33. R. L. KLUEH, P. J. MAZIASZ, I. S. KIM, L. HEATHERLY, D. T. HOELZER, N. HASHIMOTO, E. A. KENIK, and K. MIYAHARA, "Tensile and Creep Properties of an Oxide Dispersion-Strengthened Ferritic Steel," *J. Nucl. Mater.*, **307–311**, 773 (2002).

34. C. LEMAIGAN and A. T. MOTTA, "Zirconium Alloys in Nuclear Applications," Vol. 10: "Nuclear Materials," B. R. T. FROST, Ed., *Materials Science and Technology Series*, p. 1, R. W. CAHN, P. HAASEN, and E. J. CRAMER, Eds., VCH (1994).

35. M. GRIFFITHS, R. W. GILBERT, and V. FIDLERIS, "Neutron Damage in Zirconium Alloys Irradiated at 644 to 710 K," *J. Nucl. Mater.*, **150**, 159 (1987).

36. W. REIERSEN et al., *Proc. Symp. Fusion Engineering*, p. 1035, Institute of Electrical and Electronics Engineers (1998).

37. Y. SHIMOMURA et al., "ITER-FEAT Operation," *Nucl. Fusion*, **41**, 309 (2001).

38. J. D. GALAMBOS, L. J. PERKINS, S. W. HANEY, and J. MANDREKAS, "Commercial Tokamak Reactor Potential with Advanced Tokamak Operation," *Nucl. Fusion*, **35**, 551 (1995).

39. H. R. WILSON, "Bootstrap Current Scaling in Tokamaks," *Nucl. Fusion*, **32**, 257 (1992).

40. S. C. JARDIN et al., "Physics Basis for a Tokamak Fusion Power Plant," *Fusion Eng. Des.*, **48**, 281 (2000).

41. "The ITER Project L-7 Implementation," ENEA, Web site: ⟨www.brasimone.enea.it/iterl-7.htm⟩ (1998).